

# Morphodynamic instabilities of planar beaches: Sensitivity to parameter values and process formulations

M. D. Klein and H. M. Schuttelaars<sup>1</sup>

Section of Hydraulic Engineering, Delft University of Technology, Delft, Netherlands

Received 29 July 2004; revised 14 June 2005; accepted 1 July 2005; published 8 October 2005.

[1] The initial growth of bed perturbations on planar sloping beaches under the forcing of obliquely incident, breaking waves is investigated using a state-of-the-art numerical model. This allows for a systematic investigation of the sensitivity of the spatial structures of the bed perturbations and their growth and migration rates to different model formulations and parameterizations. If the sediment is only transported in the direction of the net current velocity and sediment stirring is taken proportional to the wave height squared, growing up-current oriented crescentic bars are found with a preferred spacing of 800 m and a down-current migration rate of  $10 \text{ m d}^{-1}$ . Varying the angle of wave incidence, drag coefficient and bed slope results in qualitatively similar growing bed forms. Using an Engelund and Hansen transport formula, very oblique down-current oriented bars are obtained that grow in time. No preferred wavelength, however, is found. Using the Bailard transport formula results in growing, up-current oriented bars with a preferred spacing smaller than 300 m for wave angles smaller than  $7^\circ$ . When using either the Engelund and Hansen or Bailard sediment transport formulation, it is essential to take the transport in the direction of the wave orbital velocity into account in order to have growing bed perturbations.

**Citation:** Klein, M. D., and H. M. Schuttelaars (2005), Morphodynamic instabilities of planar beaches: Sensitivity to parameter values and process formulations, *J. Geophys. Res.*, *110*, F04S18, doi:10.1029/2004JF000213.

## 1. Introduction

[2] Rhythmic bed topography is observed in a wide range of systems. On river beds, dunes and alternating bars are found, whereas the bed of a shallow shelf sea like the North Sea is covered with tidal sand banks [see, e.g., Dyer and Huntley, 1996], shoreface-connected ridges [Van de Meene and van Rijn, 2000], and sand waves and megaripples [Terwindt, 1971]. Also the topography of the surf zone of virtually any coast exhibits rhythmic features both in the shoreline and the subtidal (barred) topography. These features have been the subject of many studies. Rhythmic shoreline features range from beach cusps of  $O(10 \text{ m})$  to coastline sand waves of  $O(1000 \text{ m})$  [see, e.g., Verhagen, 1989; Stive et al., 2002; Falqués and Calvete, 2003]. Subtidal rhythmic features have length scales ranging from a few tens of meters to a few thousands of meters and consist mainly of rip channels and crescentic patterns [see, e.g., Bowen and Inman, 1971; Wright and Short, 1984; Konicki and Holman, 2000; Van Enckevort and Ruessink, 2003; Van Enckevort et al., 2004].

[3] Different theoretical explanations for the generation of rhythmic patterns in the surf zone have been given in the literature. One explanation focuses on the effects of direct hydrodynamic forcing. Bowen and Inman [1971] and Holman and Bowen [1982] show that a combination of two or more edge waves can yield net circulation cells resulting in a rhythmic topography if these edge waves have the same frequency and a certain fixed phase coupling. This phase coupling can be the result of free incident and reflected long waves on a perturbed bathymetry [see Chen and Guza, 1998].

[4] The second explanation for surf zone rhythmicity is self-organization in the coupled hydro- and morphodynamic system, as introduced by Sonu [1968]. Observations that are in favor of this explanation are rhythmic features like ripples whose length scales do not correspond with the length scales in the hydrodynamic forcing. The initial phase of self-organization can be studied by performing a linear stability analysis (LSA).

[5] Reniers et al. [2004] have presented a model incorporating both mechanisms, although, unlike Holman and Bowen [1982], sediment is not transported in the wave boundary layer. They have shown that a hydrodynamic forcing by wave groups made up of directionally spread incident short waves yields a longshore periodic topography. The spacing of these rhythmic features corresponded with the length scales of slowly varying, persisting circula-

<sup>1</sup>Also at Institute for Marine and Atmospheric Science, Utrecht University, Netherlands.

tion patterns [MacMahan *et al.*, 2004] and not with the length scales of the residual flow patterns caused by edge wave/incident wave interactions that were also present in the model. The rip channel spacing in this model depends on the directional spreading of the short waves and is of the order of 200 m. In this sense this model considers the rhythmic topography to be caused by direct hydrodynamic forcing, although the template is a stochastic process and therefore the morphology is not an exact copy of the forcing. Since feedback between the bed and the hydrodynamics can occur as well, self-organization is not excluded. This is evident from the results without directional spreading, that resulted in rhythmic bed features with longshore length scales of  $O(300)$  m.

[6] Without directional spreading the forcing is uniform and also in that case a rhythmic topography emerges. This is the result of positive feedback between an initially longshore uniform topography, “perturbed” by very small numerical rounding-off errors.

[7] A number of studies concerning linear stability analyses of planar beaches have appeared in the literature. The first study of surf zone morphology with a stability model is described by Hino [1974]. Under the forcing of obliquely incident, breaking waves, down-current oriented bars are found as fastest growing modes with a spacing of about 4 times the surf zone width  $x_b$ . A bar is defined as down-current oriented if the longshore position of the seaward tip of the bar is situated down-current (with respect to the mean longshore current) of the shoreward tip. Figure 18 in section 3.2.1 gives an example of a down-current oriented bar. Christensen *et al.* [1994] extended Hino’s study by enhancing the formulation of the physical processes like wave forcing and sediment transport. Applying a sediment transport relation accounting for bed load transport results in up-current oriented bars with a spacing of about six times the surf zone width.

[8] The influence of the angle of wave incidence, the parameterization of sediment stirring and the exponent of the current velocity in the formulation of the sediment transport are structurally explored by Falqués *et al.* [2000] and Ribas *et al.* [2003]. Falqués *et al.* [2000] focused on normal incident waves. For a sediment stirring function increasing quadratically with the distance from the shoreline and remaining constant seaward of the breaker line, crescentic patterns with alternating channels and shoals around the breaker line are found. The spacing of the fastest growing mode is about 3 to 5 times the surf zone width. Ribas *et al.* [2003] investigated, among others, the influence of the angle of wave incidence and found down-flow migrating, crescentic bar features in case of a sediment transport relation that depended linearly on the local velocity and for wave angles larger than  $5^\circ$ . For smaller angles the direction of migration alters, although the bed perturbation does not significantly change its shape.

[9] In these studies the bed changed both owing to interactions between the bed perturbations and the incident waves (the so-called bed-surf effects) and the interactions between the bed perturbations and the flow field (the so-called bed-flow effects). Falqués *et al.* [1996] focused on bed-flow interaction. They prescribed a longshore-uniform longshore current profile and studied the effects of bed-flow interaction on the linear stability characteristics of planar

beaches. For parameter values representative of natural beaches, down-current bars with a spacing of 1 to 4 times the surf zone width were found.

[10] In the linear stability analyses mentioned above, many simplifications had to be made in order to be able to linearize explicitly the hydro- and morphodynamic equations. These simplifications concern a saturated surf zone assumption, regular waves, linear bed shear stress and a simple transport formula. These simplifications are based on the assumption of wave-dominated conditions, namely, a wave orbital velocity that is much larger than the mean current velocity.

[11] The present study aims at assessing the importance of a number of these simplifications and the sensitivities of the model results to different values of the drag coefficient, the bed slope and the angle of wave incidence. Furthermore, the linear stability characteristics of planar beaches under both current-dominated and wave-dominated conditions are investigated; these regimes are covered by Falqués *et al.* [1996] and Ribas *et al.* [2003], respectively.

[12] To these ends, the stability properties of the surf zone morphology are studied using a state-of-the-art numerical model, in which different formulations and parameterizations can be chosen. Using a numerical model has three main advantages. In the first place, process simplifications do not have to be made. The second advantage is that the stability properties of any type of coast can easily be assessed; hence the model is not restricted to planar beaches. Third, the growth of bed perturbations is not restricted to initial stages only, but can be extended into the nonlinear regime, describing the temporal morphological development, while using the same model.

[13] The numerical model is referred to as the fully nonlinear model when the wave forcing is computed using a second-generation wave model, the bed shear stress formulation incorporates the effects of both currents and waves, and the sediment transport rates are computed with methods of either Engelund and Hansen [1967] or Bailard [1981]. If, on the other hand, Longuet-Higgins’ [1970] formulations for wave forcing, mixing and bed shear stress and a simplified transport formulation are used, the model is referred to as the idealized model. By comparing the results of the idealized and the fully nonlinear model, the influence of different model formulations and forcings can be studied.

[14] In section 2, the model formulations and the method to perform a linear stability analysis with a numerical model, which has already been used by Deigaard *et al.* [1999] and Klein *et al.* [2002], are discussed. The results of the linear stability analyses are presented in section 3. The discussion of these results, including a discussion of the mechanism explaining the sign of the growth rate and the overall shape of the bed perturbation obtained with the idealized model, is treated in section 4. The conclusions, finally, are drawn in section 5.

## 2. Model Formulations

[15] This section discusses the model formulations and the method used to determine the linear stability characteristics (growth and migration rates and spatial structure of the bed perturbation) of planar beaches. Figures 1 and 2 define the coordinate system and a number of the variables used in

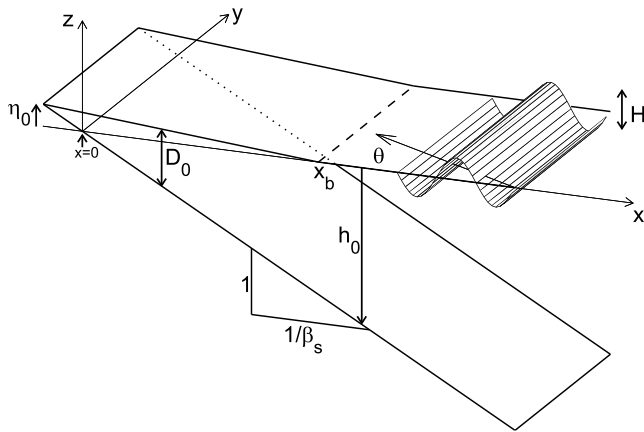


**Figure 1.** Definition sketch of the equilibrium state. For a discussion of the symbols, see the text.

this study. The coastal system that is being studied concerns a planar sloping beach with a slope  $\beta_s$ , uniform in the longshore direction  $y$ . The reference bed level is denoted by  $h_0$ . Note that  $x = 0$  is defined at the location where the still water level intersects with the reference bed profile. A bed perturbation is denoted by  $h'$  and a shoal (channel) corresponds with  $h' > 0$  ( $h' < 0$ ); see Figure 2.

[16] The water motion near the coast is forced by obliquely incident waves that break at or around  $x = x_b$ . At the breaker line the (significant) wave height  $H$  ( $H_s$ ) is denoted by  $H_b$  and the wave angle  $\theta$  by  $\theta_b$ . The exact definitions of the breaker line are given when the wave models are introduced. A number of the parameters mentioned above have been summarized in Table 1.

[17] Breaking of waves results, amongst others, in a mean wave setup, denoted in Figures 1 and 2 by  $\eta_0$ . If a bed perturbation  $h'$  is present, a perturbation in the free surface elevation  $\eta'$  exists as well. The equilibrium depth  $D_0 = \eta_0 - h_0$  is a function of the cross-shore coordinate  $x$  only and the total water depth is given by  $D = D_0 + \eta' - h'$ .

### 2.1. Fully Nonlinear Model

[18] The water motion is described by the depth- and wave-averaged shallow water equations [Phillips, 1977; Horikawa, 1999], consisting of the mass conservation equation

$$\frac{\partial \eta}{\partial t} + \frac{\partial u_c D}{\partial x} + \frac{\partial v_c D}{\partial y} = 0 \quad (1)$$

and the momentum equations

$$\begin{aligned} \frac{\partial u_c}{\partial t} + u_c \frac{\partial u_c}{\partial x} + v_c \frac{\partial u_c}{\partial y} + g \frac{\partial \eta}{\partial x} + \frac{\tau_x}{\rho_w D} - \frac{F_x}{\rho_w D} - \frac{\partial}{\partial x} \left( \nu \frac{\partial u_c}{\partial x} \right) \\ - \frac{\partial}{\partial y} \left( \nu \frac{\partial u_c}{\partial y} \right) = 0 \end{aligned} \quad (2)$$

$$\begin{aligned} \frac{\partial v_c}{\partial t} + u_c \frac{\partial v_c}{\partial x} + v_c \frac{\partial v_c}{\partial y} + g \frac{\partial \eta}{\partial y} + \frac{\tau_y}{\rho_w D} - \frac{F_y}{\rho_w D} - \frac{\partial}{\partial x} \left( \nu \frac{\partial v_c}{\partial x} \right) \\ - \frac{\partial}{\partial y} \left( \nu \frac{\partial v_c}{\partial y} \right) = 0 \end{aligned} \quad (3)$$

in which  $t$  is time,  $\eta = \eta_0 + \eta'$  the free surface elevation,  $x$  ( $y$ ) the cross-shore (longshore) coordinate,  $u_c$  ( $v_c$ ) the cross-shore (longshore) current velocity,  $D$  the total water depth,  $g$  the acceleration of gravity,  $\tau_x$  and  $\tau_y$  the bed shear stresses,  $F_x$  and  $F_y$  the wave forces per surface area,  $\rho_w$  the water density and  $\nu$  the turbulent eddy viscosity, which is assumed to be uniform with a default value of  $1 \text{ m}^2 \text{ s}^{-1}$ . These equations are solved numerically using the Delft3D modeling system [see Roelvink and van Banning, 1994].

[19] The bed shear stresses are computed with the formulations proposed by Fredsøe [1984], incorporating the effects of waves and currents on both the direction and the magnitude of the bed shear stress. In the numerical model, the parameterization of Soulsby *et al.* [1993] of these formulations is used.

[20] Propagation, refraction and breaking of obliquely incident, irregular short waves are computed with the second-generation wave model HISWA [Holthuijsen *et al.*, 1989] which is based on an evolution equation of the wave action density spectrum,

$$\frac{\partial N c_{g,x}}{\partial x} + \frac{\partial N c_{g,y}}{\partial y} + \frac{\partial N c_{g,\theta}}{\partial \theta} = -D_w, \quad (4)$$

in which the wave action  $N$  is defined as the variance density  $E$  [ $\text{m}^2 \text{ Hz}^{-1}$ ] divided by the wave frequency  $\phi$ . Furthermore,  $c_{g,x}$ ,  $c_{g,y}$  [ $\text{m s}^{-1}$ ] and  $c_{g,\theta}$  [ $\text{rads}^{-1}$ ] are the propagation speeds of wave action in the  $x$ ,  $y$  and angular space, and  $\theta$  is the wave angle.  $D_w$  [ $\text{m}^2 \text{ s}^{-1}$ ] is the wave action dissipation, computed with the breaker model of Battjes and Janssen [1978], calibrated by Battjes and Stive [1985]. This energy dissipation is distributed over the direction bins, proportional to the existing directional energy distribution. In HISWA, a maximum wave height is computed, either with the breaker height coefficient  $\gamma$  (depth-induced breaking) or with a parameter controlling steepness-induced breaking. This maximum wave height is used to compute the fraction of breaking waves. Note that the breaker height coefficient  $\gamma$ , the parameter that has to be defined in

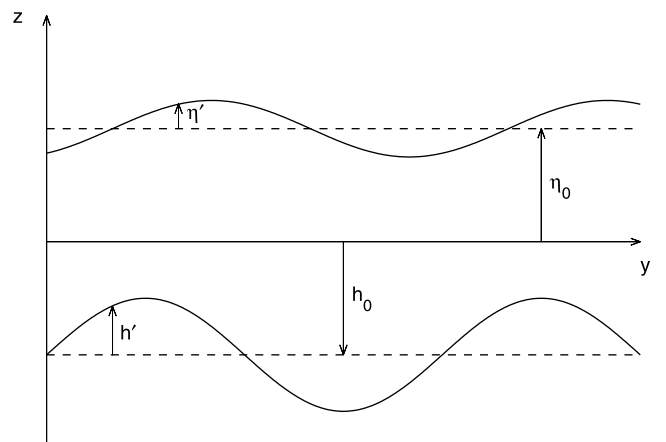


**Figure 2.** Definition sketch of the perturbed state (longitudinal section). For a discussion of the symbols, see the text.

**Table 1.** Default Parameter Values Used in the Numerical Experiments

Parameter	Symbol	Value	Unit
<i>Idealized Model</i>			
Wave height	$H_b$	0.78	m
Breaker depth	$D_b$	0.97	m
Breaker parameter	$\gamma_b$	0.8	
Turbulence coefficient	$N$	0.01	
Length model domain	$L_y$	12000	m
<i>Fully Nonlinear Model</i>			
Significant wave height	$H_s$	1.1	m
Breaker height coefficient	$\gamma$	0.8	
Eddy viscosity	$\nu$	1	$\text{m}^2 \text{s}^{-1}$
Length model domain	$L_y$	6000	m
<i>General</i>			
Wave angle at breaking	$\theta_b$	5	deg
Bed slope	$\beta_s$	0.01	
Drag coefficient	$c_d$	0.0035	
Gravitational acceleration	$g$	9.81	$\text{m s}^{-2}$
Water density	$\rho_w$	1030	$\text{kg m}^{-3}$
Sediment density	$\rho_s$	2650	$\text{kg m}^{-3}$
Median grain size	$D_{50}$	250	$\mu\text{m}$
Porosity	$n$	0.4	
Width model domain	$L_x$	1200	m
Cross-shore grid size	$dx$	10	m
Longshore grid size	$dy$	10	m

HISWA, is not equal to the breaker parameter  $\gamma_b$ , defined as  $H_b/h_b$ . The dissipation is used to compute the wave forces  $\vec{F}$  per surface area with the formulation proposed by *Dingemans et al.* [1987],

$$\vec{F} = \rho_w g D_w \phi \vec{k}. \quad (5)$$

A consequence of this formulation of the wave stresses is that no water level set-down is computed in the shoaling zone. When using HISWA, the breaker line is defined as the location of maximum wave energy dissipation.

[21] The sediment transport vector  $\vec{q}$  is computed using either the *Bailard* [1981] or the *Engelund and Hansen* [1967] formulations. The *Bailard* [1981] formulation, which is appropriate in case of wave-dominated conditions, reads when the bed slope terms are omitted,

$$\vec{q} = \vec{q}_b + \vec{q}_s = \frac{f_{cw} \epsilon_b}{g(s-1) \tan \phi_i} \|\vec{u}\|^2 \vec{u} + \frac{f_{cw} \epsilon_s}{g(s-1) w_s} \|\vec{u}\|^3 \vec{u}, \quad (6)$$

in which  $f_{cw}$  is a friction factor taking into account the friction due to waves and currents,  $\epsilon_b$  ( $\epsilon_s$ ) the efficiency factor for bed (suspended) load,  $s$  the relative density  $\rho_s/\rho_w$  with  $\rho_s$  the density of the sediment,  $\phi_i$  the angle of repose and  $w_s$  the sediment fall velocity. Bed slope effects are neglected since they are small and since, according to *Ribas et al.* [2003], the results of linear stability analyses of planar beaches are robust under changes of the bed slope parameter, accounting for bed slope effects.

[22] Defining  $\vec{u} = \vec{u}_c + \vec{u}_0 \sin(\phi t)$  with  $\phi$  the (peak) frequency of the short wave,  $\vec{u}_c = (u_c, v_c)$  and  $\vec{u}_0$  the

amplitude of the wave orbital velocity, the formulations for wave-averaged bed load  $\vec{q}_b$  and suspended load  $\vec{q}_s$  read

$$\vec{q}_b = \frac{f_{cw} \epsilon_b}{g(s-1) \tan \phi_i} \left[ \left( u_c^2 + v_c^2 + \frac{1}{2} u_0^2 + \frac{1}{2} v_0^2 \right) \vec{u}_c + \left( u_c u_0 + v_c v_0 \right) \vec{u}_0 \right] \quad (7)$$

$$\vec{q}_s = \frac{f_{cw} \epsilon_s}{g(s-1) w_s} \left( (u^2 + v^2)^{3/2} \vec{u} \right). \quad (8)$$

The first term between the square brackets of equation (7) is associated with the bed load transport in the direction of the mean current, whereas the second term corresponds to the bed load transport in the direction of the wave orbital motion. In equation (8) the time averaging over the wave period, denoted by brackets, is done numerically. See *van der Molen* [2002] for more details.

[23] When studying current-dominated conditions, sediment transport can be described using the *Engelund and Hansen* [1967] formulation for the total load. In this formulation, the sediment transport reads

$$\vec{q} = a \vec{u}^5 \quad (9)$$

with

$$a = \frac{0.05}{\sqrt{g} C^3 (s-1)^2 D_{50}}. \quad (10)$$

Here  $C$  is the Chézy coefficient and  $D_{50}$  the median grain size. Averaging equation (9) over a wave cycle results in the following expression, in which the sediment transport is divided in a part in the direction of the mean current and a part in the direction of the wave orbital velocity near the bed:

$$\vec{q} = \alpha_c(x, y) \vec{u}_c + \alpha_w(x, y) \vec{u}_0. \quad (11)$$

The complete expressions of the sediment stirring functions  $\alpha_c(x, y)$  and  $\alpha_w(x, y)$  read

$$\alpha_c(x, y) = \frac{a}{8} \left[ 8u_c^4 + 3u_0^4 + 8v_c^4 + 32u_c u_0 v_c v_0 + 24v_c^2 v_0^2 + 3v_0^4 + 8u_c^2 (3u_0^2 + 2v_c^2 + v_0^2) + u_0^2 (8v_c^2 + 6v_0^2) \right] \quad (12)$$

$$\alpha_w(x, y) = \frac{a}{2} \left[ 4u_c^3 u_0 + 4u_c^2 v_c v_0 + u_c u_0 (3u_0^2 + 4v_c^2 + 4u_c^3 + 3v_0^2) + v_c v_0 (3u_0^2 + 4v_c^2 + 4u_c^3 + 3v_0^2) \right]. \quad (13)$$

The sediment mass conservation equation reads

$$(1-n) \frac{\partial h}{\partial t} = -\vec{\nabla} \cdot \vec{q} \quad (14)$$

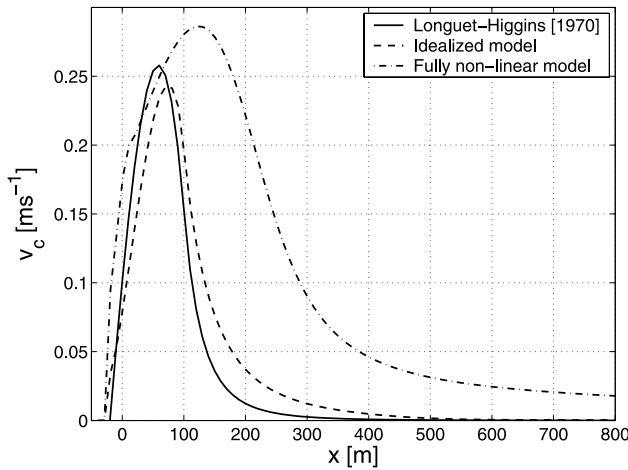


**Figure 3.** Longshore current velocity profiles, according to *Longuet-Higgins* [1970] and obtained with the idealized and fully nonlinear model. The settings of the reference experiment has been used; see Table 1.

and states that the bed changes are due to divergences and convergences of the sediment fluxes. Bed porosity is denoted by  $n$ .

## 2.2. Idealized Model

[24] In order to assess the importance of different parameterizations and formulations, the governing equations of the above described fully nonlinear model are simplified using a number of assumptions. Using the shallow water approximation, the magnitude of the wave orbital velocity  $u_0$  is given by  $0.5\gamma_b\sqrt{gD}$  with  $\gamma_b = H_b/D_b$  the wave breaker parameter. With  $\gamma_b = 0.8$  and choosing a breaker wave height  $H_b$ , the depth  $D_b$  at which waves break and the position of the breaker line are defined. Now assuming (1) a small angle of wave incidence and (2) a magnitude of the mean velocity  $\bar{u}_c$  much smaller than the magnitude of the wave orbital velocity  $u_0$ , the bed shear stress terms can be expressed as [see *Dodd*, 1994]

$$\tau_x = \frac{4}{\pi}\rho_w c_d u_0 u_c \quad (15)$$

$$\tau_y = \frac{2}{\pi}\rho_w c_d u_0 v_c, \quad (16)$$

in which  $c_d$  is the drag coefficient.

[25] Furthermore, the *Longuet-Higgins* [1970] formulations for the wave forcing and mixing are used instead of applying a second-generation wave model and a constant eddy viscosity. In the work of *Longuet-Higgins* [1970], the turbulent eddy viscosity  $\nu(x)$  is defined as  $Nx\sqrt{gD}$ , with  $N$  an empirical coefficient. Unlike *Longuet-Higgins*' formulations,  $\nu(x)$  is exponentially decaying outside the surf zone. For details, see *Ribas et al.* [2003].

[26] Here the *Engelund and Hansen* [1967] transport formulation is chosen in order to be able to compare with results obtained in the literature, for example, those of *Falqués et al.* [1996] and *Ribas et al.* [2003]. Using assumption 2, neglecting the sediment transport in the

direction of the wave orbital velocity and averaging in longshore direction, the *Engelund and Hansen* [1967] sediment transport formulation of equation (9) reduces to

$$\bar{q} = \frac{3a}{128}(g\gamma_b H)^2 \bar{u}_c \equiv \alpha(x)\bar{u}_c. \quad (17)$$

## 2.3. Morphodynamic Equilibrium

[27] Choosing a longshore-uniform bottom profile, equations (1) to (4) allow for a solution that is longshore-uniform and time independent. This holds for both the idealized and the fully nonlinear model. From the mass conservation equation it follows that the cross-shore velocities are zero. Then equations (2) and (3) reduce to

$$g \frac{\partial \eta}{\partial x} - \frac{F_x}{\rho_w D} = 0 \quad (18)$$

$$\frac{\tau_y}{\rho_w D} - \frac{F_y}{\rho_w D} - \frac{\partial}{\partial x} \left( \nu \frac{\partial v_c}{\partial x} \right) = 0. \quad (19)$$

In cross-shore direction the wave forcing is balanced by the pressure term, resulting in a longshore-uniform wave setup. In longshore direction, the bed shear stress, wave forcing and mixing term balance each other, driving an longshore-uniform current. The longshore current velocity profiles associated with the longshore-uniform bottom profile according to the theory of *Longuet-Higgins* [1970] and those computed with the idealized and the fully nonlinear model are displayed in Figure 3. It is clear that, although the theoretical profile and the profile resulting from the idealized model are quite similar, differences remain. The main differences are due to the formulation of the viscosity profile (see section 2.2) and the fact that in the idealized model a wave setup is present only within the breaker zone, whereas *Longuet-Higgins* redefined the bed slope due to wave setup even outside the breaker zone. Differences in the longshore current velocity profile of the idealized and the fully nonlinear model are mainly due to the different wave models that have been used.

[28] In case of the linear sediment transport relation as used in the idealized model (equation (17)), the sediment transport in cross-shore direction associated with the longshore-uniform beach is zero, since the cross-shore velocities are zero. The longshore sediment transport is longshore-uniform, like the longshore current. This means that the divergences and convergences of the sediment transport are zero, and hence do not lead to any bed changes. Therefore any longshore-uniform bathymetry is an equilibrium bathymetry. In the fully nonlinear model, it is assumed that the longshore-uniform part of the sediment transport in the direction of the wave orbital motion (equation (11)) is compensated by offshore sediment transport processes like undertow, and hence that the unperturbed coastal system is in equilibrium.

## 2.4. Linear Stability Analysis

[29] The standard way to study the linear stability of a morphodynamic equilibrium is by adding a small perturbation, which is periodic in longshore direction, to this

equilibrium and linearizing the equations with respect to this small perturbation. This results in an eigenvalue problem. Solving this eigenvalue problem results in the eigenfunction with corresponding growth and migration rates. The eigenfunction describes the spatial structure of the perturbed quantities. The growth rate indicates whether this perturbation exponentially grows or decays in time. The migration rate indicates the direction in which and the celerity with which the perturbation migrates. However, in this study the formal linearization of the governing equations cannot be performed since a numerical model is used to compute the perturbed radiation stresses, velocity field and free surface elevation for a given bed perturbation. The implication of this is that another method for solving the stability problem has to be used. This method has been introduced by *Deigaard et al.* [1999].

[30] The method used starts with an initial guess of the spatial structure of the bed perturbation, with a certain longshore wave number and a cross-shore amplitude distribution. This bed perturbation can both grow and migrate in time and can be written as

$$h' = \beta(x) \exp[i(ky - \omega t)] + c.c., \quad (20)$$

in which  $i$  is the imaginary unit,  $k = 2\pi/\lambda$  the longshore wave number of the bed perturbation,  $\beta(x) = \beta_r(x) + i\beta_i(x)$  the complex cross-shore amplitude function and  $\omega = \omega_r + i\omega_i$  with  $\omega_r$  being the migration rate and  $\omega_i$  the growth rate. Note that at this moment both the spatial cross-shore amplitude distribution  $\beta(x)$  and the complex eigenvalue  $\omega$  are yet to be determined.

[31] Using an initial guess for the bed perturbation with wavelength  $\lambda$ , the wave forces are computed. With these forces the flow field and water levels are computed. This is repeated a number of times until the interactions between the waves and the free surface elevation are correctly taken into account. The final stationary flow field is used to compute the sediment transport rates and the corresponding bed changes. The divergence of the sediment transport, associated with the wavelength  $\lambda$  under consideration, are retrieved by means of a Fourier decomposition and can be written as

$$-\nabla \bar{q} = \Lambda(x) \exp[iky] + c.c. \quad (21)$$

Using equation (14), with  $\partial h/\partial t$  evaluated using equation (20), evaluated at  $t = 0$  (hence considering initial bed changes), and equation (21) finally yields the Rayleigh quotient  $R$  [see *Griffel*, 1985],

$$R = \frac{\int_0^\infty \Lambda(x)\beta(x)^* dx}{\int_0^\infty \beta(x)\beta(x)^* dx} = -i\omega, \quad (22)$$

with  $*$  indicating the complex conjugate. The function  $\Lambda(x)$  is used as a new guess for the cross-shore amplitude function of the bed perturbation, and the procedure sketched above is repeated, resulting in a new  $\Lambda(x)$  and  $R$ . This process is repeated until  $R$  does not change from one iteration to the next. When this procedure has converged,

$\Lambda(x)\exp[iky]$  is the eigenfunction, defining the spatial structure of the bed perturbation and  $R$  contains the information about the eigenvalue, with  $\omega_i = \text{Re}(R)$  and  $\omega_r = -\text{Im}(R)$ .

[32] In this procedure only one longshore wavelength is considered. The procedure yields the most unstable or least stable solution associated with this wavelength. Repeating this procedure for a range of wavelengths, one is able to find the wavelength with the largest growth rate. If this maximum growth rate is positive, the mode associated with it is the fastest growing mode (FGM). The wavelength of the FGM is denoted as  $\lambda_p$  and the corresponding growth and migration rate as  $\omega_{i,p}$  and  $\omega_{r,p}$ , respectively.

[33] Note that the fully nonlinear equations are used to calculate the perturbed radiation stresses and water motion. Hence, in principle, nonlinear interactions are taken into account as well. However, by choosing the amplitude of the bed perturbation sufficiently small, the nonlinear contributions are negligible. This can easily be verified by looking at the ratios of the amplitudes of the velocity components resulting from nonlinear interactions (i.e., components with longshore wavelengths not equal to the wavelength under study) and the amplitude of the velocity components associated with wavelength under study. This ratio should be small. If a maximum amplitude of 0.01 m is used, the ratio is of the order  $1e^{-3}$  and hence nonlinear components are indeed negligible.

[34] Owing to the use of a numerical model and the iterative procedure to obtain the eigenvalues and eigenfunctions, the range of wavelengths that can be considered is limited. The lower limit is 300 m, since the above described iteration process does not converge for wavelengths smaller than approximately 300 m and hence no results are obtained. The upper limit is determined by the length of the model domain. Although the model domain is at least 6000 m, the maximum wavelength that can be assessed is approximately 3000 m, since the area of interest has to be well away from the disturbances induced by the lateral model boundaries.

### 3. Numerical Results

[35] This section describes the results of the linear stability analyses (LSAs) performed with both the idealized (section 3.1) and the fully nonlinear model (sections 3.2 and 3.3). In the discussion of the results of the idealized model, a reference experiment with parameters representative of natural beaches (Table 1) is defined and discussed (section 3.1.1). The default significant wave height is about the yearly-averaged significant wave height observed along the Dutch coast. The default angle of wave incidence is based on the work of *Falqués et al.* [1996] and *Ribas et al.* [2003]. All other parameters have physically feasible values. Only the parameters deviating from these reference settings are included in the captions of the figures presenting the results.

[36] To be able to easily characterize the hydrodynamic conditions observed in the experiments, a parameter  $\gamma_{cw}$  is introduced,

$$\gamma_{cw} = \frac{v_{c,m} - u_{0,b}}{v_{c,m} + u_{0,b}}, \quad (23)$$

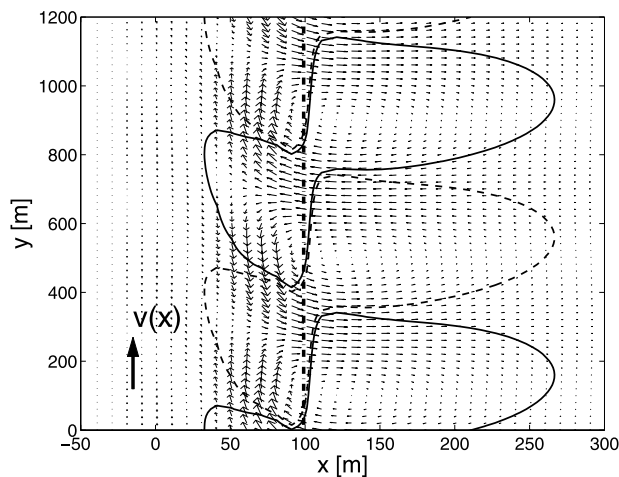


**Figure 4.** Bed and flow perturbations of the FGM ( $\lambda_p = 800$  m) of the reference experiment performed with the idealized model. Here  $v(x)$  denotes the direction of the unperturbed longshore current.

where  $v_{c,m}$  is the maximum velocity of the mean longshore current and  $u_{0,b}$  is the wave orbital velocity at the breaker line, computed with the linear wave theory. If  $\gamma_{cw} \simeq 1$ ,  $v_{c,m} \gg u_{0,b}$  and the hydrodynamic conditions can be characterized as current-dominated. If, on the other hand,  $\gamma_{cw} \simeq -1$ ,  $v_{c,m} \ll u_{0,b}$  and hence the hydrodynamic conditions are wave-dominated. In practice, however,  $\gamma_{cw}$  varies roughly between  $-0.8$  and  $-0.3$ .

[37] The sensitivities of the linear stability characteristics to variations in the drag coefficient, the bed slope and the angle of wave incidence are explored in section 3.1.2. The last experiment in this section discusses the effects of irregular waves and wave refraction with respect to the perturbed bathymetry by coupling the idealized model to the HISWA wave model.

[38] Next, the sensitivity of the results to bed-flow and bed-surf interactions is investigated in section 3.1.3 by adjusting process formulations. First of all, the effects of bed-surf and bed-flow interactions is investigated, while using the idealized sediment transport formulation of equation (17). Perturbations in the radiation stresses result from bed and water level perturbations. By omitting these perturbations from the wave forcing terms, a longshore-uniform longshore current is obtained that only interacts with the bed via bed-flow interaction, similar to *Falqués et al.* [1996]. From a hydrodynamic point of view, this condition is current-dominated.

[39] Then the standard hydrodynamic formulations (i.e., including the bed and water level perturbations in the wave forcing) are applied in combination with a wave-dominated sediment stirring function  $\alpha_c^{wd}(x)$ , obtained from  $\alpha_c(x, y)$  in equation (11) after averaging in the longshore direction. Thence  $\alpha_c^{wd}(x)$  is associated with the morphodynamic equilibrium state. Note that the sediment that is available owing to this wave-dominated sediment stirring function is transported in the current direction only.

[40] In the next series of experiments, these wave-dominated conditions are changed into current-dominated conditions by varying the hydrodynamic conditions from

wave-dominated to current-dominated by gradually excluding the bed and water level perturbations in the wave forcing terms and by changing the sediment stirring function from the wave-dominated stirring function  $\alpha_c^{wd}$  to the current-dominated stirring function  $\alpha_c^{cd}$ . This  $\alpha_c^{cd}$  function is obtained from equation (11) by neglecting the wave orbital velocity and averaging in longshore direction. In the final experiment, the sediment stirring function  $\alpha_c^{wd}(x)$  is used in combination with radiation stresses calculated using HISWA instead of those derived by *Longuet-Higgins* [1970].

[41] It is important to note that there are two essential differences between the latter experiment (HISWA and  $\alpha_c^{cd}(x)$ ) and the experiments of section 3.2, which are performed with the fully nonlinear model coupled to the *Engelund and Hansen* [1967] sediment transport formulation. The first difference is that in section 3.2 the sediment stirring function is a function of both the longshore and the cross-shore coordinate instead of being longshore-uniform. Second, in the fully nonlinear model sediment is transported in the direction of both the wave orbital and current velocity, while in the model presented in section 3.1.3 the transport in the direction of the wave orbital velocity is neglected. Another difference is the (non)linearity of the bed shear stress. However, it has been shown by *Klein and Schuttelaars* [2004] that whether the bed shear stress is linear or not does not essentially influence the results of the LSA.

[42] In section 3.2, a reference experiment, using the parameters given in Table 1, has been performed with the fully nonlinear model coupled to the *Engelund and Hansen* [1967] sediment transport formulation. The sensitivities of that model to variations in parameter values have been investigated. The importance of different contributions to the sediment transport within the *Engelund and Hansen* [1967] formulations is investigated as well. In section 3.3, finally, the same experiments as presented in section 3.2 are performed with the nonlinear model coupled to the *Bailard* [1981] sediment transport formula.

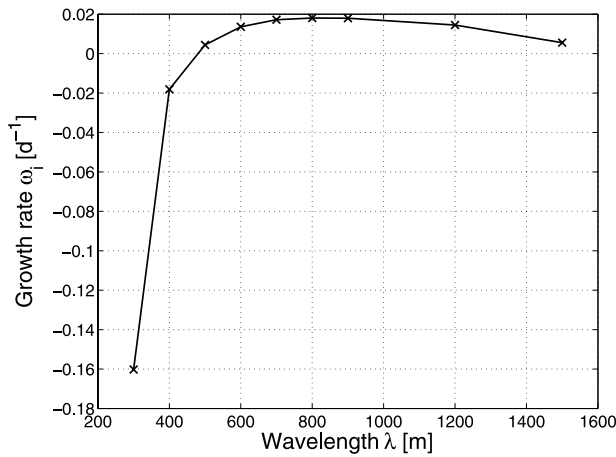
[43] Unless stated otherwise, the results concern the fastest growing modes (FGM), i.e., the eigenfunctions with the largest growth rate. In general, the spacing of the FGM has been determined with an accuracy of 100 m. When necessary, the increment has been reduced to 10 m.

### 3.1. Results of the Idealized Model

#### 3.1.1. Reference Experiment

[44] Figure 4 shows the spatial structure of the bed perturbation of the FGM obtained with the idealized model, using the default parameter settings (see Table 1). In this and all other experiments, the direction of the unperturbed longshore current (indicated in Figure 4 by  $v(x)$ ) is such that the coast is on the left when looking in the direction of the mean current. The magnitude of the longshore current is  $0.25 \text{ m s}^{-1}$  and the amplitude of the wave orbital velocity at the breaker line is  $1.24 \text{ m s}^{-1}$ . Hence  $\gamma_{cw} = -0.67$ , indicating that the hydrodynamics in this experiment are wave-dominated.

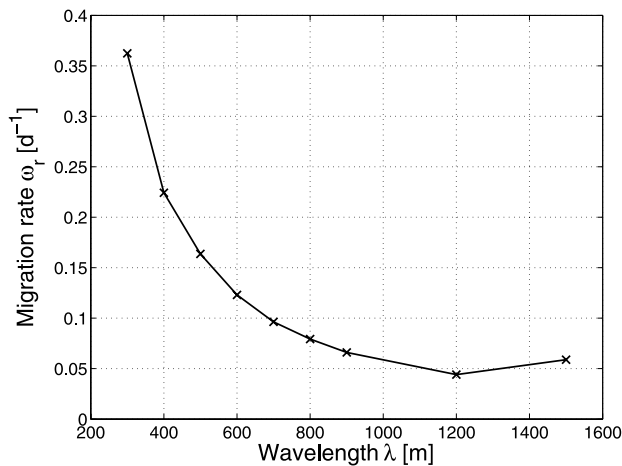
[45] The wavelength of the FGM is 800 m. The eigenfunction, describing the spatial structure of the bed perturbation, is a crescentic pattern with alternating shoals (solid contours) and channels (dashed contours) around the



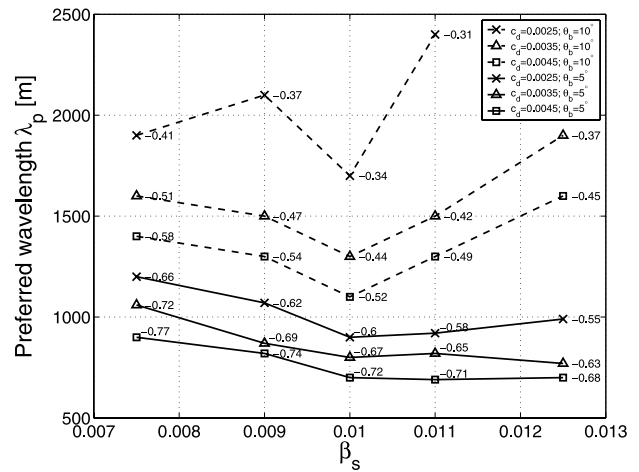
**Figure 5.** Growth rate of the reference experiment performed with the idealized model as a function of the longshore wavelength.

breaker line, indicated by the straight dash-dotted line. The bar at the seaward side of the breaker line, called the outer bar, is perpendicular to the shoreline, whereas the inner bar is up-current oriented. A bar is up-current oriented if the longshore position of the seaward tip of the bar is situated up-current (with respect to the mean longshore current) of the shoreward tip. The perturbed flow pattern, depicted in Figure 4 as well, is a circulation pattern that is slightly shifted in longshore direction with respect to the bed perturbation; that is, the location of maximum cross-shore velocity in the surf zone is situated somewhat down-current of the location with a maximum amplitude of the bed perturbation. Nevertheless, in the surf zone mainly an onshore current is present on top of a shoal and an offshore current exists over a channel, and vice versa outside the surf zone.

[46] Figure 5 depicts the growth rate of the bed perturbations for different longshore wavelengths. It clearly shows that a maximum growth rate occurs for  $\lambda = \lambda_p = 800$  m. This maximum is positive, meaning that the bed perturba-



**Figure 6.** Migration rate of the reference experiment performed with the idealized model as a function of the longshore wavelength.



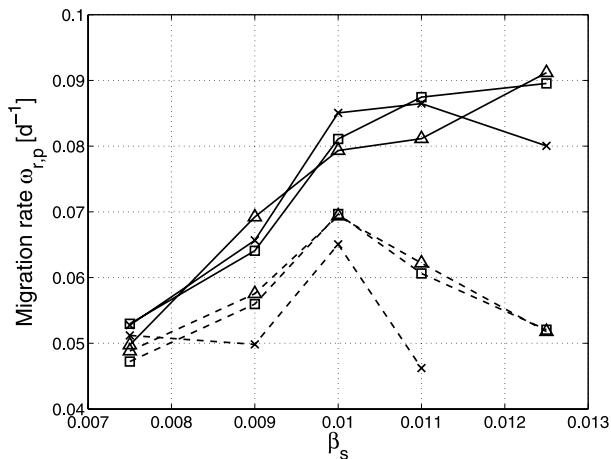


**Figure 9.** Sensitivity of the migration rates of the FGM to the drag coefficient  $c_d$ , the bed slope  $\beta_s$  and the angle of wave incidence  $\theta_b$ . The numbers in Figure 7 represent  $\gamma_{cw}$ . Other parameters have default values (Table 1). Results are obtained with the idealized model. For the legend, see Figure 7.

0.010, 0.011 and 0.0125), three drag coefficients (0.0025, 0.0035 and 0.0045) and two angles of wave incidence ( $5^\circ$  and  $10^\circ$ ). Note that when varying  $\beta_s$  the position of the breaker line is changed, since both the wave height and the breaker parameter are kept fixed.

[48] The results, as far as the wavelength  $\lambda_p$ , the growth rate  $\omega_{i,p}$  and the migration rate  $\omega_{r,p}$  of the FGM are concerned, are plotted in Figures 7, 8 and 9. No results are presented for the combination of  $\beta_s = 0.0125$ ,  $c_d = 0.0025$  and  $\theta_b = 10^\circ$  because no FGM is found for wavelengths up to 3000 m, the maximum wavelength that can be assessed with this model.

[49] The influence of friction, the angle of wave incidence and the bed slope on  $\lambda_p$  is shown in Figure 7. For every FGM, the parameter  $\gamma_{cw}$  is plotted as well. The smaller the drag coefficient and the larger the angle of wave incidence, the less wave-dominated the hydrodynamic conditions are and the larger the preferred spacing  $\lambda_p$ . This dependence is independent of the bed slope.

[50] The influence of the bed slope on  $\lambda_p$ , on the contrary, is not straightforward. A minimum in the wavelength exists for a slope of approximately 1% for  $\theta_b = 10^\circ$ . This minimum is less pronounced if the water motion becomes more wave-dominated and eventually disappears for small angle and large friction, although a local minimum in the preferred spacing is still present at  $\beta_s = 0.01$ .

[51] In Figure 8 the dependence of the growth rate of the FGM on the drag coefficient, the bed slope and the angle of wave incidence is presented. It clearly shows that increasing the angle of wave incidence results in smaller growth rates. The dependence of the growth rate on the drag coefficient is more complex. For  $\theta_b = 5^\circ$  no clear trend independent of the bed slope and the angle of wave incidence is found, whereas for  $\theta_b = 10^\circ$  the growth rate seems to increase with increasing  $c_d$ . Interestingly enough, a maximum growth rate is found for a bed slope of 1%, independent of the angle of wave incidence and the drag coefficient.

[52] From Figure 9 it is clear that the sensitivities of the migration rates to the bed slope depend on the angle of wave incidence as well. For a large angle, a maximum in the migration rate is again found for a bed slope of 1%. For a small angle of wave incidence, the migration rate increases with increasing bed slope. For both wave angles, however, no clear trend between the migration rate and the drag coefficient is visible.

[53] The spatial structures of the bed and flow perturbations have the same characteristics as the one of the reference experiment presented in Figure 4, although on a detailed level differences in the orientation and the cross-shore extent exist.

[54] The effects of refraction with respect to the perturbed bathymetry and irregular waves are assessed by coupling the idealized model to HISWA instead of using that of Longuet-Higgins [1970]. In the HISWA model, a breaker height coefficient of 0.8 has been applied, which is a good compromise to match both the location and the magnitude of maximum longshore current velocity with those following from the idealized model forced with the Longuet-Higgins [1970] formulations. Owing to irregularity of the waves, a significant wave height  $H_s$  has to be defined. A significant wave height of 1.1 m in deep water has been used which corresponds, according to the Rayleigh distribution, to a wave height of 0.78 m in the idealized model. The bed slope  $\beta_s$  is set to 0.0075, while the other parameters have their default values (see Table 1). With these settings and the application of HISWA,  $\gamma_{cw} = -0.82$ .

[55] Using HISWA, a preferred spacing of 700 m is found. This is much smaller than the wavelength of 1060 m obtained in the experiments with the wave forcing according to the formulation of Longuet-Higgins [1970]; see Figure 7. The spatial structure of the bed perturbation is quite similar, but both the growth and migration rates decrease. Varying the breaker height coefficient shows that a larger  $\gamma$  yields a larger maximum longshore current velocity and a narrower surf zone, resulting in a smaller preferred spacing. The opposite is true for a smaller  $\gamma$ . This dependence of the preferred spacing on the longshore current velocity corresponds with the fact that  $\gamma_{cw} = -0.82$ . The hydrodynamics are wave-dominated and therefore the effects of the waves are more important for the linear stability characteristics than the longshore current.

### 3.1.3. Sensitivity to the Sediment Stirring Function

[56] By omitting the bed and water level perturbations from the radiation stresses, a model very similar to that of Falqués *et al.* [1996] is obtained, in which bed-surf interactions are omitted. Note that the unperturbed radiation stresses still result in a longshore current. With this model the current-dominated regime has been explored. The sediment stirring  $\alpha(x)$  that has been used, is the same one as used in the idealized model and is proportional to the wave height squared (see equation (17)). Owing to the saturated surf zone assumption, wave heights are linearly decreasing through the surf zone and constant beyond, resulting in a discontinuous  $\alpha(x)$ ; see the solid line in Figure 10. With the current-dominated hydrodynamics and a sediment stirring function proportional to the wave height squared, growing bed features are found with the growth rate increasing with decreasing wavelength. Hence no FGM has been found for wavelengths larger than 300 m. The bed and flow perturba-

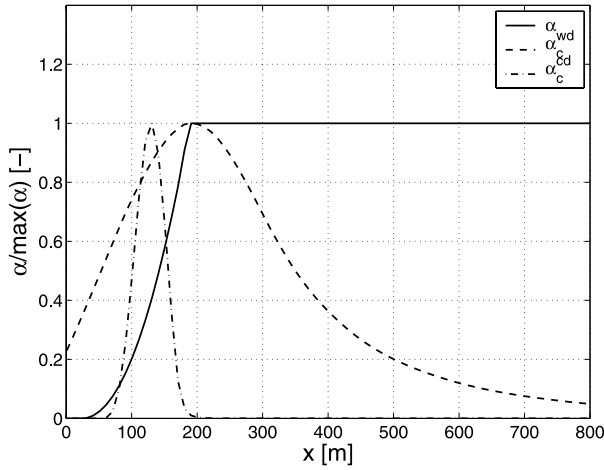


**Figure 10.** Sediment stirring functions  $\alpha(x)$  (solid line),  $\alpha_c^{wd}$  (dashed line) and  $\alpha_c^{cd}$  (dash-dotted line).

tions associated with  $\lambda = 400$  m are depicted in Figures 11 and 12. The spatial structure of the bed perturbation is quite different from the one found in the reference experiment: The orientation of the inner bar changes from up-current in the reference experiment to down-current in the current-dominated situation.

[57] Next, the current-dominated and wave-dominated regimes are explored not only by adjusting the hydrodynamic formulations as described above but also by adjusting the sediment stirring functions. Using equation (11), neglecting the transport in the direction of the wave orbital velocity and only retaining the sediment stirring associated with the morphodynamic equilibrium, a wave-dominated sediment stirring function  $\alpha_c^{wd}$  is obtained. This stirring function, scaled with its maximum value, is depicted in Figure 10 with a dashed line and is defined in equation (11).

[58] The current-dominated stirring function  $\alpha_c^{cd}$ , depicted in Figure 10 with the dash-dotted line after scaling with its maximum value, is obtained from equation (11) by assuming  $\vec{u}_0 \ll \vec{u}_c$  and by averaging in longshore direction (associated with the unperturbed bathymetry). Therefore

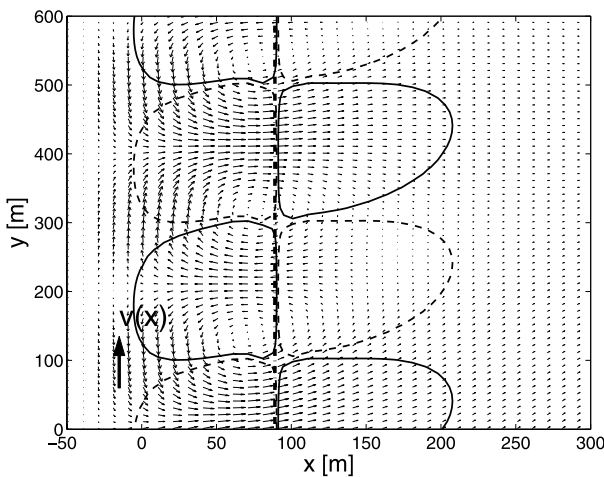


**Figure 11.** Bed and flow perturbations with a wavelength of 400 m for a current-dominated situation ( $\gamma_{cw} = 1$ ). The applied sediment stirring function is  $\alpha(x)$ .

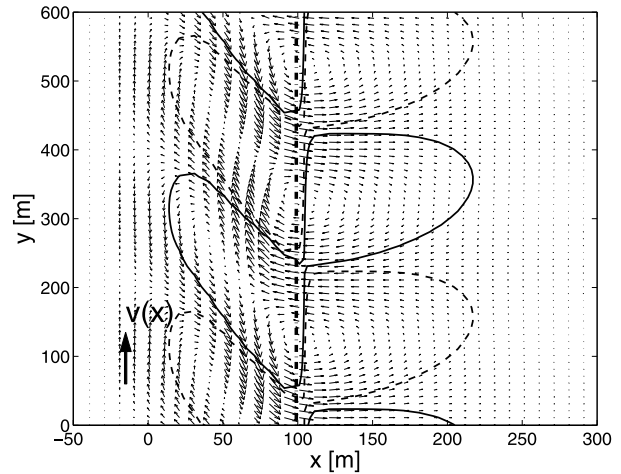


**Figure 12.** Bed and flow perturbations with a wavelength of 400 m for a wave-dominated situation ( $\gamma_{cw} = -0.67$ ). The applied sediment stirring function is  $\alpha(x)$ .

the longshore-uniform, current-dominated sediment stirring  $\alpha_c^{cd}$  is proportional to  $v_c^4$ .

[59] In Figure 13 the growth rates are plotted as a function of the longshore wavelength, with ‘x’ denoting results obtained using  $\alpha_c^{wd}(x)$  and considering wave-dominated hydrodynamics, and ‘Δ’ denoting the results obtained using  $\alpha_c^{cd}(x)$  and considering current-dominated hydrodynamics. For  $\alpha_c^{wd}(x)$ , Figure 13 shows that the growth rate increases with increasing wavelength, but never reaches a maximum value. In fact, the growth rates of all wavelengths considered (up to 2900 m) are negative. Using  $\alpha_c^{cd}$ , Figure 14 shows that bed perturbation has changed into a down-current oriented bar instead of an undulating pattern of alternating shoals and troughs along the breaker line. The perturbed flow structure is a circulation pattern with mainly onshore flow over the shoals and offshore flow above the troughs.

[60] The results obtained with  $\alpha_c^{cd}(x)$  are similar to the results obtained with current-dominated hydrodynamics and a sediment stirring function proportional to the wave height

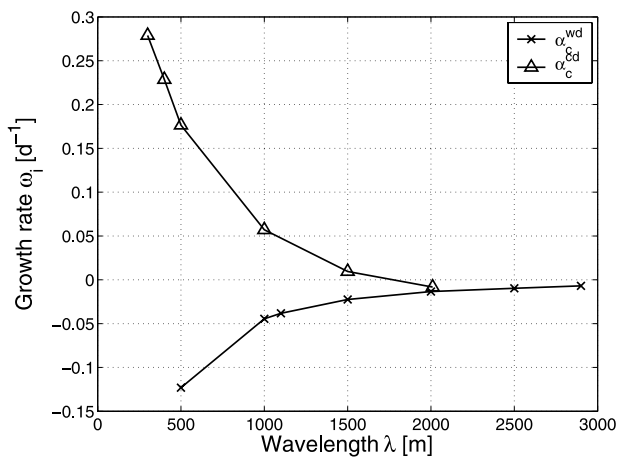


**Figure 13.** Growth rate versus wavelength using  $\alpha_c^{wd}$  and  $\alpha_c^{cd}$ . Results are obtained with the idealized model. Here  $\beta_s = 0.0075$ ; other parameters have default values.

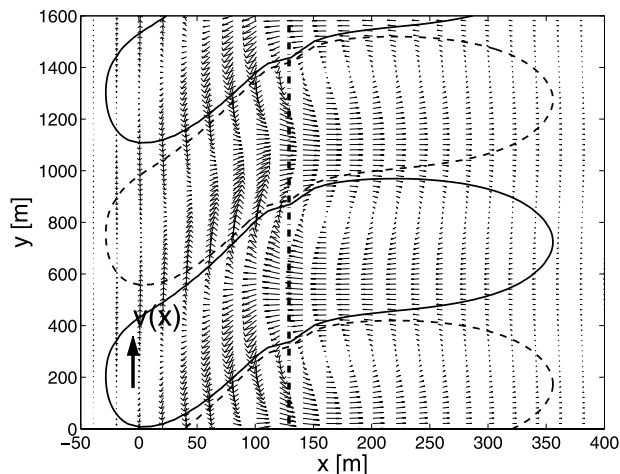


**Figure 14.** Bed and flow perturbations obtained with  $\alpha_c^{wd}$ . Results are obtained with the idealized model. Here  $\beta_s = 0.0075$ ; other parameters have default values.

squared: the growth rate increases with decreasing wavelength and no FGM is found for wavelengths larger than 300 m (Figure 13). Also the spatial structure (see Figure 15) is virtually the same, namely, an undulating crescentic pattern with down-current oriented inner bars.

[61] An additional experiment has been performed in which the idealized model, using  $\alpha_c^{wd}$ , is coupled to HISWA. The effects of a more sophisticated wave forcing and  $\alpha_c^{wd}$  on the bed perturbation are similar to the results of the idealized model without HISWA (see Figure 13). The bar is still down-current oriented with mainly onshore flow over the shoals, whereas the growth rates are negative and increase with increasing wavelength.

### 3.2. Results of the Fully Nonlinear Model Coupled to the Engelund and Hansen [1967] Sediment Transport Formula

#### 3.2.1. Reference Experiment and Parameter Sensitivity

[62] Applying the fully nonlinear model coupled to the transport formula of Engelund and Hansen [1967] and

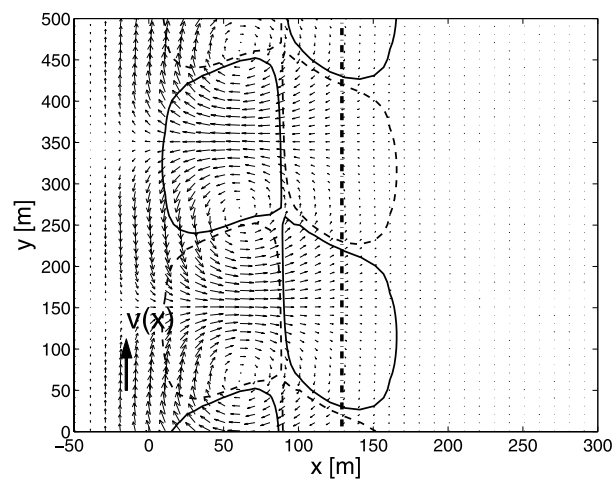


**Figure 15.** Bed and flow perturbations obtained with  $\alpha_c^{cd}$ . Results are obtained with the idealized model. Here  $\beta_s = 0.0075$ ; other parameters have default values.

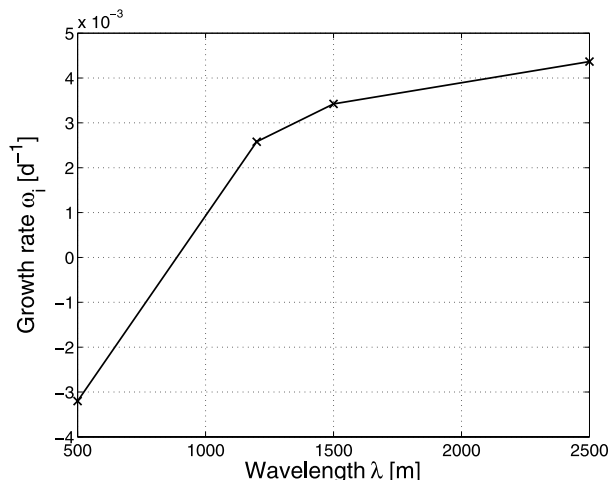


**Figure 16.** Growth rate of the reference experiment performed with the fully nonlinear model coupled to the Engelund and Hansen [1967] sediment transport formulation as a function of the longshore wavelength.

using the default parameter settings (see Table 1), the growth and migration rates as a function of the longshore wavelength are shown in Figures 16 and 17, respectively. The growth rate increases from negative values for small wavelengths to positive values for large wavelengths. However, no FGM is found in the range of wavelengths considered. The migration rate is decreasing with increasing wavelength and is positive, meaning down-flow migrating bed features.

[63] The resulting bed perturbations can be characterized as very oblique down-current oriented bars. Figures 18 and 19 demonstrate that the obliqueness of the bars increases with increasing wavelength. These figures furthermore demonstrate that with increasing wavelength the current velocity perturbations become shore-parallel, whereas for small wavelengths a clear circulation pattern with onshore flow over the shoals and offshore flow above the troughs can be observed (compare Figure 4 obtained with

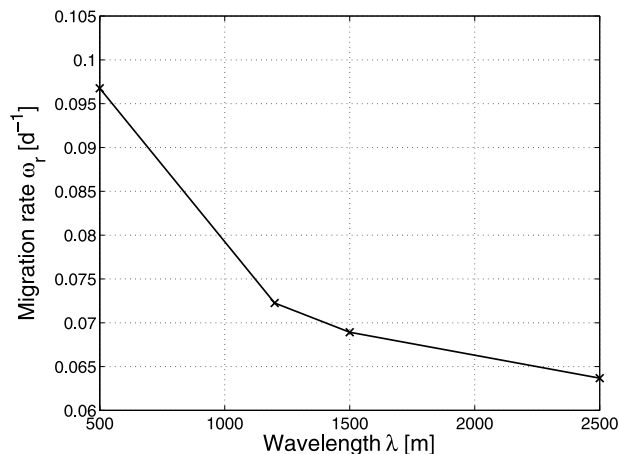


**Figure 17.** Migration rate of the reference experiment performed with the fully nonlinear model coupled to the Engelund and Hansen [1967] sediment transport formulation as a function of the longshore wavelength.

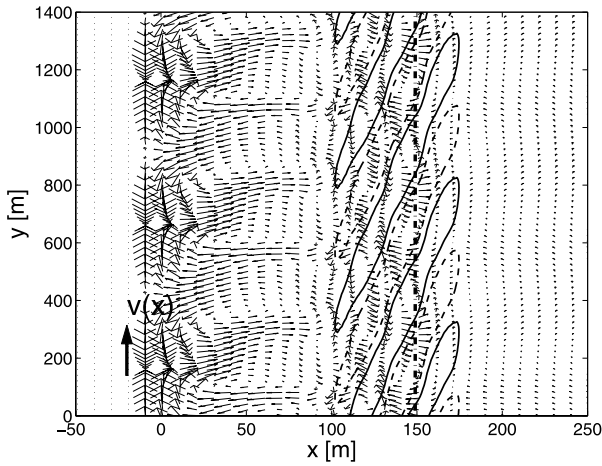


**Figure 18.** Bed and flow perturbations associated with  $\lambda = 500$  m. The breaker line, defined in section 2.1, is indicated by the straight dash-dotted line. Here  $\gamma_{cw} = -0.47$ .

the idealized model). Note that no bed perturbations near the coastline emerge, despite the fact that velocities with comparable magnitude as near the breaker line are present. This is due to the fact that the sediment stirring close to the shoreline is insignificant, and hence the amplitude of the bed perturbation near the coastline is negligible compared to the amplitude of the bed perturbation around the breaker line.

[64] The dependence of these results on the drag coefficient and the bed slope has been investigated as well by performing LSAs for  $c_d = 0.0025$  and  $0.0045$  with  $\beta_s = 0.01$ , and for  $\beta_s = 0.0075$  and  $0.0125$  with  $c_d = 0.0035$ . Irrespective of the value of the drag coefficient or the bed slope, the dependence of the growth and migration rates on the longshore wavelength is similar to the dependence found for the reference experiment, namely, increasing growth rate and decreasing migration rate with increasing longshore wavelength. Hence also for varying  $c_d$  and  $\beta_s$  no FGM are found. Also the bed perturbations are similar, namely, very

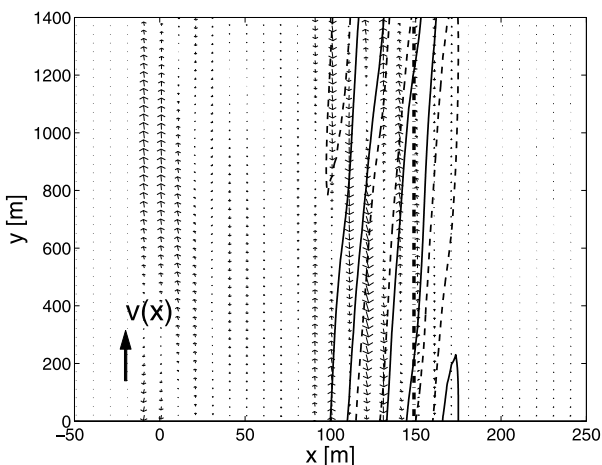


**Figure 19.** Bed and flow perturbations associated with  $\lambda = 2500$  m. The breaker line, defined in section 2.1, is indicated by the straight dash-dotted line. Here  $\gamma_{cw} = -0.47$ .

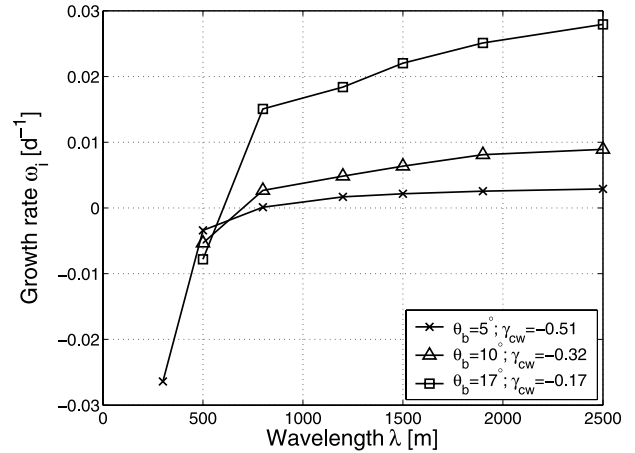


**Figure 20.** Sensitivity of the growth rate to the longshore wavelength and the angle of wave incidence  $\theta_b$ . Here  $\beta_s = 0.0075$ , other parameters have default values. Results are obtained with the fully nonlinear model coupled to the *Engelund and Hansen* [1967] sediment transport formula.

oblique down-current oriented bars, which become more oblique with increasing wavelength and thus with increasing growth rate.

[65] The migration rate and the absolute value of the growth rate decrease with increasing  $c_d$ . As observed in the previous section, the growth rates have a maximum value for a bed slope of 1%. For steep slopes, only decaying bed forms are found. The migration rate decreases with decreasing bed slope.

### 3.2.2. Sensitivity to the Angle of Wave Incidence

[66] The sensitivity of the growth and migration rate to the angle of wave incidence has been investigated by considering three angles of wave incidence, namely,  $\theta_b =$

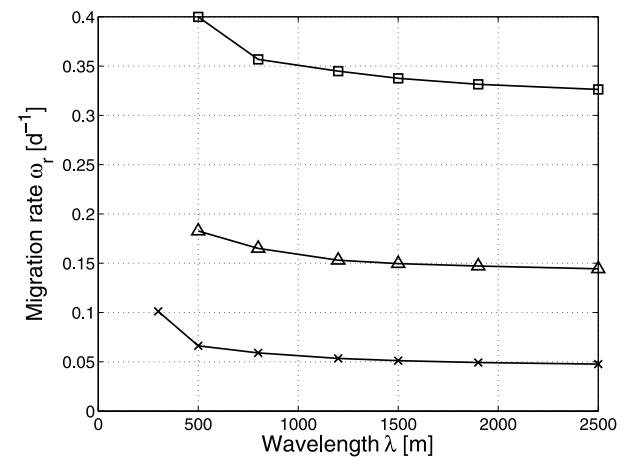


**Figure 21.** Sensitivity of the migration rate to the longshore wavelength and the angle of wave incidence  $\theta_b$ . Here  $\beta_s = 0.0075$ , other parameters have default values. Results are obtained with the fully nonlinear model coupled to the *Engelund and Hansen* [1967] sediment transport formula.

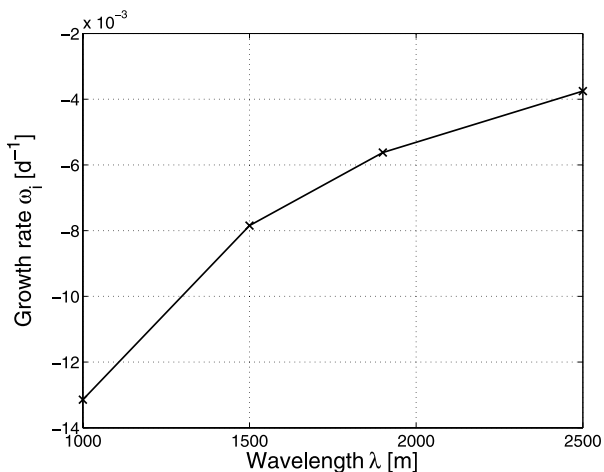


**Figure 22.** Growth rate as a function of the longshore wavelength. Results obtained with the fully nonlinear model coupled to the *Engelund and Hansen* [1967] sediment transport formulation. Only the transport in the current direction is taken into account. Here  $\beta_s = 0.0075$ , other parameters have default values;  $\gamma_{cw} = -0.51$ .

5, 10 and 17°. The results are presented in Figures 20 and 21.

[67] It is evident that the growth rate increases with increasing wave angle. Again, no FGM has been found. The results suggest that given a certain wavelength, a critical angle of wave incidence exists below which no growing features are found. The migration rate increases with increasing wave angle as well, and decreases with increasing wavelength. For large wavelengths, the migration rate hardly depends on the longshore wavelength, which is in accordance with the results obtained in the previous section. The bed perturbations have the same characteristics as described in section 3.2.1, namely, very oblique down-

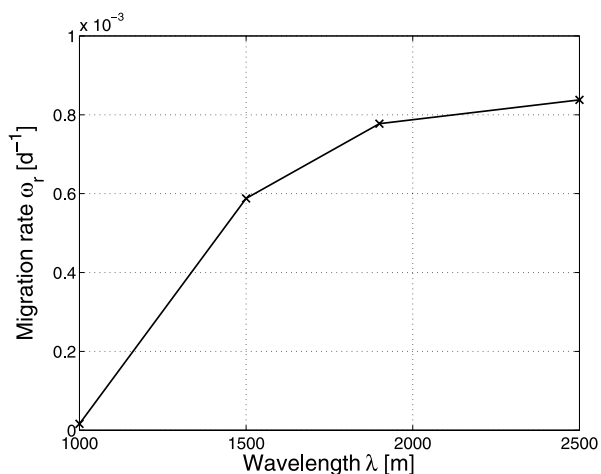


**Figure 23.** Migration rate as a function of the longshore wavelength. Results obtained with the fully nonlinear model coupled to the *Engelund and Hansen* [1967] sediment transport formulation. Only the transport in the current direction is taken into account. Here  $\beta_s = 0.0075$ ; other parameters have default values;  $\gamma_{cw} = -0.51$ .

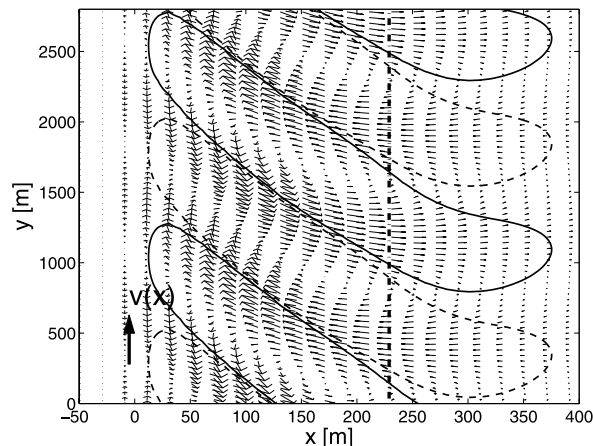


**Figure 24.** Bed and flow perturbations associated with  $\lambda = 1000$  m. Results obtained with the fully nonlinear model coupled to the *Engelund and Hansen* [1967] sediment transport formulation. Only the transport in the current direction is taken into account. Here  $\beta_s = 0.0075$ ; other parameters have default values;  $\gamma_{cw} = -0.51$ .

current bars, whose obliqueness increases with increasing growth rate.

### 3.2.3. Importance of the Various Sediment Transport Contributions

[68] In section 3.1.3 it is demonstrated that the linear stability characteristics obtained with the idealized model are sensitive to the sediment stirring function. In that section, the sediment transport formulation of the idealized model only consisted of sediment transport in the direction of the mean current. In order to investigate the importance of the sediment transport in the wave and current direction when considering the results of the fully nonlinear model, an experiment has been performed in which the contribution of the sediment transport in the direction of the waves has been omitted. The only essential difference with the last

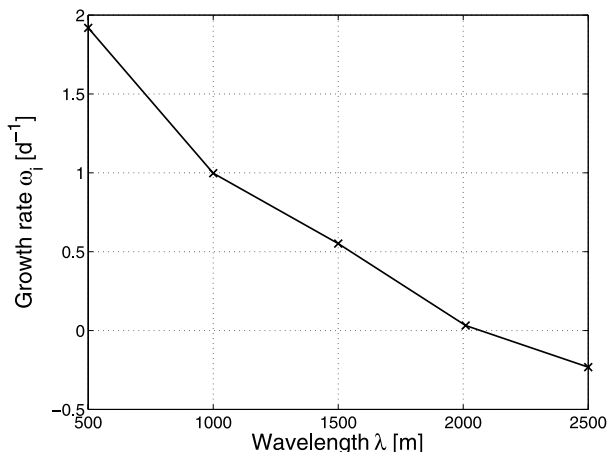


**Figure 25.** Growth rate as a function of the longshore wavelength of the reference experiment performed with the fully nonlinear model coupled to the *Bailard* [1981] sediment transport formulations. Here  $\gamma_{cw} = -0.47$ .

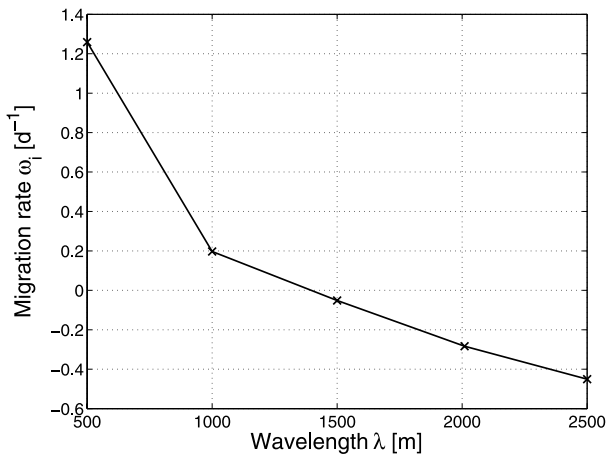


**Figure 26.** Migration rate as a function of the longshore wavelength of the reference experiment performed with the fully nonlinear model coupled to the *Bailard* [1981] sediment transport formulations. Here  $\gamma_{cw} = -0.47$ .

experiment described in section 3.1.3 is the dependence of the wave stirring function on both the cross-shore and longshore coordinate whereas in section 3.1.3 the wave stirring function is averaged over the longshore coordinate.

[69] Figures 22, 23 and 24 depict the results obtained with the fully nonlinear model and the *Engelund and Hansen* [1967] transport formulation excluding the contribution in the direction of the wave orbital motion. Decaying, up-current oriented bed forms are found and although the growth rate increases with increasing wavelength, it never becomes positive but approaches zero. Furthermore, the migration rate increases with increasing wavelength and is positive. From a comparison with section 3.2.1 it is evident that the contribution of the sediment transport in the direction of the waves is crucial for (1) having linearly growing bed forms, (2) the orientation of the bars and

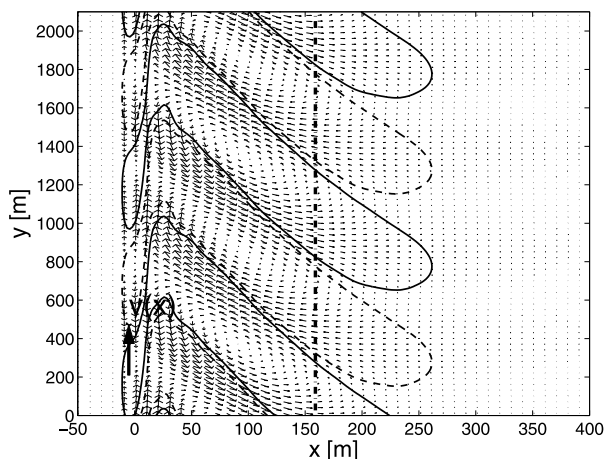


**Figure 27.** Bed and flow perturbations associated with  $\lambda = 1000$  of the reference experiment performed with the fully nonlinear model coupled to the *Bailard* [1981] sediment transport formulations. Here  $\gamma_{cw} = -0.47$ .

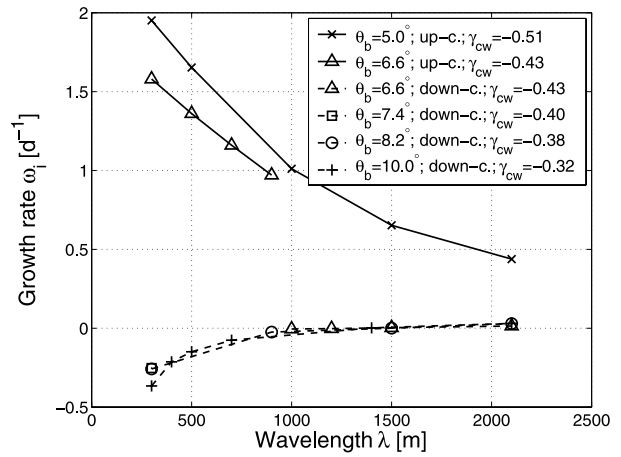


**Figure 28.** Growth rate as a function of the longshore wavelength and the angle of wave incidence  $\theta_b$ . Here  $\beta_s = 0.0075$ , other parameters have default values. Results are obtained with the fully nonlinear model coupled to the *Bailard* [1981] sediment transport formulations. Dashed lines correspond with up-current (up-c) bars, solid lines correspond with down-current (down-c) bars.

(3) the dependence of the migration rate on the wavelength.

### 3.3. Results of the Fully Nonlinear Model Coupled to the *Bailard* [1981] Sediment Transport Formula

#### 3.3.1. Reference Experiment and Parameter Sensitivity

[70] With the application of the *Bailard* [1981] sediment transport formulations in combination with the fully nonlinear model, the results of the LSA change dramatically compared to the results obtained with the *Engelund and Hansen* [1967] formulations. The results of an experiment with reference settings (see Table 1) are plotted in Figures 25, 26 and 27. Both the growth and the migration

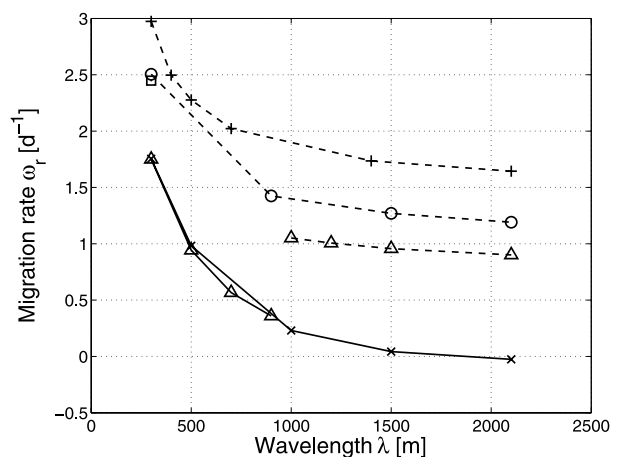


**Figure 29.** Migration rate as a function of the longshore wavelength and the angle of wave incidence  $\theta_b$ . Here  $\beta_s = 0.0075$ , other parameters have default values. Results are obtained with the fully nonlinear model coupled to the *Bailard* [1981] sediment transport formulations. Dashed lines correspond with up-current (up-c) bars, solid lines correspond with down-current (down-c) bars.

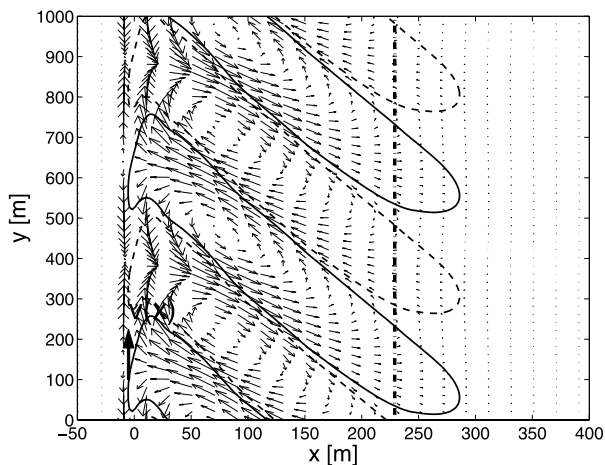


**Figure 30.** Bed and flow perturbation corresponding to  $\lambda = 500$  m and  $\theta_b = 5^\circ$ . Here  $\beta_s = 0.0075$ ; other parameters have default values. Results are obtained with the fully nonlinear model coupled to the *Bailard* [1981] sediment transport formulations.

rate decrease with increasing wavelength, being positive for small and negative for large wavelengths. No FGM has been found in the range of wavelengths under consideration.

[71] Figure 27 presents a characteristic bed perturbation, showing that up-current oriented bed features are found. Note that the bed and flow perturbations are very similar to the ones found in section 3.2.3.

[72] The same variations of the drag coefficient and the bed slope as applied in section 3.2.1, are applied here to investigate the sensitivity of the results to these parameters. Although the results on a detailed level show significant variation, generally the growth and migration rates decrease with increasing wavelength and hence no FGM is obtained for wavelengths larger than 300 m. For a fixed wavelength smaller than approximately 1000 m, a maximum growth rate is found for a bed slope of 1%. For wavelengths larger

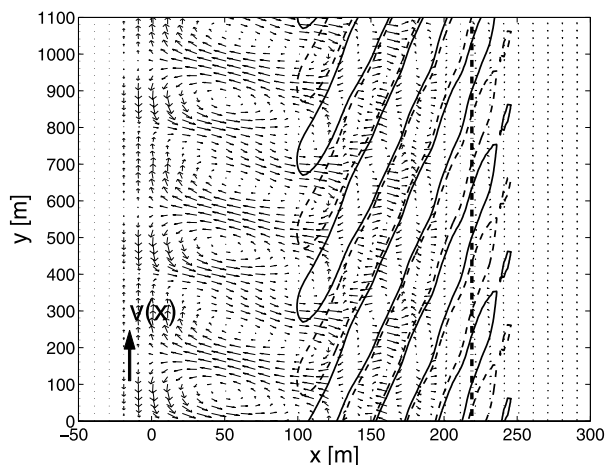


**Figure 31.** Bed and flow perturbation corresponding to  $\lambda = 500$  m and  $\theta_b = 10^\circ$ . Here  $\beta_s = 0.0075$ ; other parameters have default values. Results are obtained with the fully nonlinear model coupled to the *Bailard* [1981] sediment transport formulations.

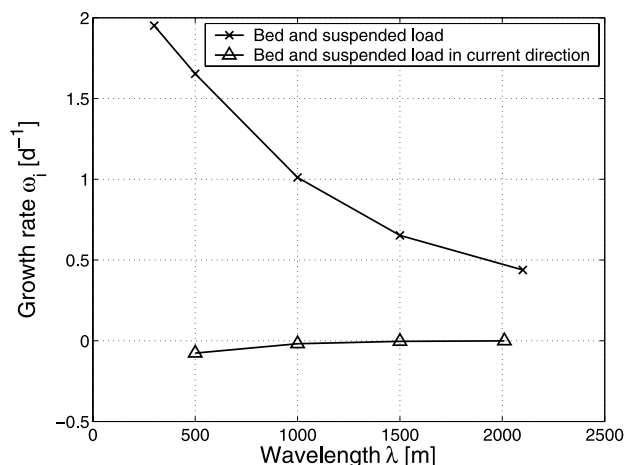


**Figure 32.** Sensitivity of the growth rate to different sediment transport modes of the *Bailard* [1981] sediment transport formulations. Here  $\beta_s = 0.0075$ ; other parameters have default values. Results are obtained with the fully nonlinear model.

than 1000 m, the growth rate decreases with increasing bed slope. The migration rate decreases with increasing friction for wavelengths smaller than 1500 m. For wavelengths larger than 1500 m, the direction of migration has altered. For wavelengths larger than 1000 m the migration rates decrease with increasing bed slope and are mainly negative, meaning up-current migration bed features. Despite these variations of the growth and migration rates, the bed and flow perturbations are robust under changes of the bed slope and the drag coefficient and are similar to the one shown in Figure 27, namely, up-current bars with mainly onshore flow over the shoals.

### 3.3.2. Sensitivity to the Angle of Wave Incidence

[73] The sensitivity of the linear stability characteristics to the angle of wave incidence is displayed in Figures 28, 29, 30 and 31. For wave angles smaller than approximately  $7^\circ$  the growth rate is a decreasing function of the wavelength, whereas the growth rates are positive for all considered wavelengths. In that case, the bed perturbation is an up-current bar; see Figure 30.

[74] For larger angles, on the contrary, the growth rate is an increasing function of the wavelength, whereas only for the larger wavelengths small but positive growth rates are found. For larger wave angles, the bed perturbation is a very oblique down-current bar; see Figure 31. These latter results are very similar to the results obtained with the fully nonlinear model coupled to the *Engelund and Hansen* [1967] sediment transport formulations.

[75] From Figure 28 it is evident that  $\theta_b = 6.6^\circ$  is a critical angle. The bed perturbations associated with  $\lambda \leq 900$  m are up-current oriented bars with the growth rate a decreasing function of the wavelength. For  $\lambda \geq 1000$  m, down-current bars are found. Hence two different modes with distinctive growth rates are found. In the range  $900 \leq \lambda \leq 1000$  m the numerical method to find the FGM converges very slowly or not at all. This is to be expected since in this range of wavelengths two distinct eigenfunctions exist with similar growth rates. The method employed to find the FGM assumes that the growth rates of the various eigenfunctions

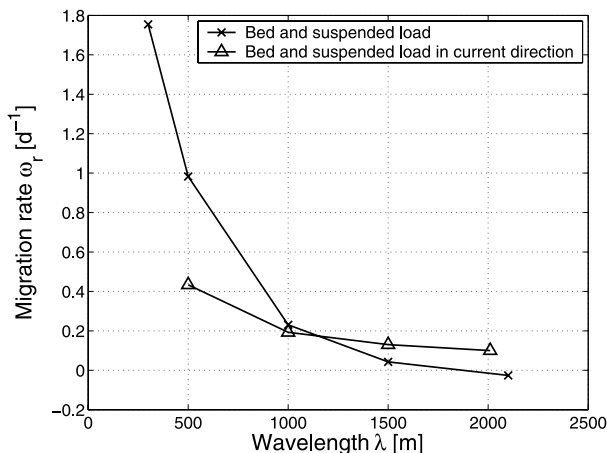


**Figure 33.** Sensitivity of the migration rate to different sediment transport modes of the *Bailard* [1981] sediment transport formulations. Here  $\beta_s = 0.0075$ ; other parameters have default values. Results are obtained with the fully nonlinear model.

are well-separated which is obviously not the case anymore. Thence the solutions in the range  $900 \leq \lambda \leq 1000$  m cannot be calculated.

[76] Irrespective of the angle of wave incidence, the migration rate is a decreasing function of the longshore wavelength. The down-current oriented modes, however, have larger migration rates than the up-current modes. Nonetheless, the migration rates are generally positive, meaning down-flow migrating bed perturbations, and increase with increasing angle of wave incidence.

### 3.3.3. Importance of the Various Sediment Transport Contributions

[77] To assess the importance of the sediment transport in the direction of the mean current, an experiment has been performed in which the contribution of the sediment transport in direction of the wave orbital motion has been omitted. Together with the reference experiment, the results are presented in Figures 32, 33 and 34. It clearly shows that omitting the sediment transport in the direction of the waves yields decaying, up-current oriented bed forms (Figure 34).

[78] A more detailed analysis shows that when sediment is only transported as bed load (i.e., neglecting suspended load) or only as suspended load (by neglecting bed load) smaller growth rates are found than those resulting from the complete *Bailard* [1981] formulations. The qualitative picture does not change, namely, positive growth rates which decrease with increasing wavelength. In case of bed load transport only, transport in the direction of the waves (current) results in growing (decaying) bed forms.

## 4. Discussion

### 4.1. Idealized Model

[79] The physical mechanism that leads to growth or decay of bottom perturbations in the surf zone has been introduced by *Falqués et al.* [1996] and is used in a number of studies, among others, those of *Falqués et al.* [2000], *Caballeria et al.* [2002] and *Ribas et al.* [2003]. To analyze

the growth or decay of a bed perturbation the so-called bottom evolution equation (BEE) is derived by using the mass conservation equation (1), the sediment transport formula (9) and the sediment mass conservation equation (14) (see *Falqués et al.* [1996] for details). Perturbations in the free surface are assumed to be negligible compared to perturbations in the bed level. Furthermore, in the derivation of the BEE it is assumed that the sediment stirring function  $\alpha$  is a function of the cross-shore coordinate only, neglecting the longshore periodic perturbations of the sediment stirring. Since this requirement is only met in case of the idealized model (see section 2.2), the BEE is only derived for the sediment transport proportional to  $\vec{u}_c$  (see equation (17)) and reads

$$\frac{\partial h'}{\partial t} + \frac{\alpha V_0}{D_0} \frac{\partial h'}{\partial y} = -\alpha \frac{\partial}{\partial x} \left( \ln \frac{\alpha}{D_0} \right) u'_c. \quad (24)$$

Here  $D_0$  is the equilibrium water depth,  $V_0$  the equilibrium longshore current velocity and  $\alpha$  is the sediment stirring function (see equation (17)), proportional to  $H^2$ . The second term on the left-hand side only results in migration, whereas the term on the right-hand side can result in growth of bed forms. The function  $\alpha/D_0$  is called the potential stirring function, following *Falqués et al.* [2000].

[80] It is obvious that a bed perturbation grows when a shoal ( $h' > 0$ ) accretes ( $\partial h'/\partial t > 0$ ) and when a channel ( $h' < 0$ ) erodes ( $\partial h'/\partial t < 0$ ). In the experiments with the idealized model,  $\alpha$  inside the surf zone is proportional to  $(\gamma_b^2 D_0)^2$  resulting in  $\partial \ln(\alpha/D_0)/\partial x > 0$ ; that is, the potential stirring inside the surf zone is increasing in offshore direction. Since  $\alpha$  is constant outside the surf zone,  $\partial \ln(\alpha/D_0)/\partial x < 0$ , or in words, the potential stirring outside the surf zone is decreasing in offshore direction. Hence, for bed perturbations to grow, the cross-shore velocity above a shoal in the surf zone must be negative (i.e., onshore directed) and positive

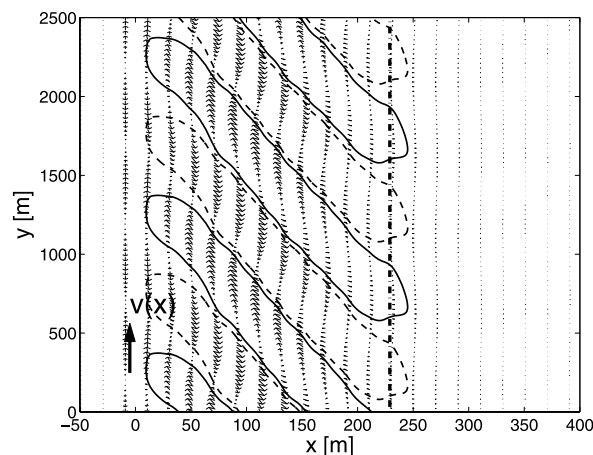


**Figure 34.** Bed and flow perturbations corresponding to  $\lambda = 1000$  m:  $\beta_s = 0.0075$ ; other parameters have default values. Results are obtained with the fully nonlinear model in which only bed and suspended load in current direction is accounted for.

(offshore directed) over a channel. Outside the surf zone, an unstable system requires offshore flow over a shoal and onshore flow over a trough. Looking at the bed and flow perturbations obtained with the idealized model and their corresponding growth rates, it is clear that the model results satisfy these requirements. Note that these arguments are only valid in case of a wave-dominated conditions.

[81] Using equation (24), the occurrence of a FGM (see, e.g., Figure 5) in the results of the idealized model can be understood. For very large wavelengths in the longshore direction, equation (1) reduces in leading order to  $(D_0 u'_c)_x = 0$  (compare section 2.3). Using the fact that the cross-shore velocity must disappear for large  $x$ , it follows that  $u'_c \rightarrow 0$  as  $\lambda \rightarrow \infty$ . On the other hand, for very small wavelengths, viscous effects are dominant in the momentum equations. In leading order in  $k$  ( $k$  is the wave number  $2\pi/\lambda$ ) equation (2) reduces to  $\nu k^2 u'_c = 0$ , showing that for large  $k$  the cross-shore velocity becomes zero. Hence for both large- and small-scale bed perturbations the perturbed velocities become zero, which implies, using equation (24), that the growth rates go to zero as well. Therefore, if a non-zero growth rate is found, either a minimum or a maximum growth rate must exist.

[82] The occurrence of a maximum growth rate as a function of bed slope  $\beta_s$  (see Figure 8) can be understood by considering planar sloping beaches with large and small bed slopes. Note that in the experiments with varying bed slope the wave height, and hence the breaker depth, are not changed. This means that the position of the breaker line varies with varying  $\beta_s$ . Scale the water depth with  $D_b$ , the cross-shore coordinate with  $D_b/\beta$  and use that, according to *Longuet-Higgins* [1970], the velocity scales with  $\beta_s$  (where the maximum of the unperturbed longshore current velocity has been used as a typical velocity). From this scaling it can be assessed that  $\partial h'/\partial t$  is of the order of  $\beta_s^2$ , implying that for  $\beta_s \rightarrow 0$  the growth rate goes to zero. Hence without a bed slope, the continuity mechanism on which equation (24) is based results in decaying perturbations. When  $\beta_s$  is very large, it can be shown that in leading order the perturbations in the free surface elevation and the bed perturbation balance. This results in a cross-shore velocity that is proportional to  $\partial h'/\partial x$  and scales with  $1/\beta_s^2$ . Since the right-hand side of equation (24) is of order  $\beta_s^2$ ,  $\partial h'/\partial t \sim \partial h'/\partial x$  in leading order in  $\beta_s$ . This results in migrating bed perturbations with zero growth rate. Hence the growth rate goes to zero for both steep and gently sloping beaches. A maximum or minimum growth rate must exist since a non-zero growth rate is found in the numerical experiments. It has to be remarked that this analysis applies to limiting values of  $\beta_s$ . The results have shown that the dependence on  $\beta_s$  is complex and depends on the angle of wave incidence as well.

[83] The occurrence of a crescentic bed perturbation with channels and shoals opposite to each other along the breaker line (see Figure 4) can be understood by looking into the sign of  $\partial \ln(\alpha/D_0)/\partial x$ . For growing bed perturbations with a shoal in the surf zone, there is always onshore flow ( $u'_c < 0$ ). The function  $\partial \ln(\alpha/D_0)/\partial x$  changes sign across the breaker line owing to the discontinuity in the sediment stirring function. Since  $u'_c$  is still mainly onshore directed on the seaward side of the breaker line, the bed perturbation must have a negative sign on the seaward side of the breaker line.

The same reasoning applies to cross sections containing a channel in the surf zone, resulting in a crescentic bed perturbation.

[84] In section 3.1.3 the sensitivity of the linear stability characteristics to the hydrodynamic conditions is investigated. Irrespective of the hydrodynamic conditions, the flow  $u'_c$  over a shoal ( $h' > 0$ ) is always onshore directed. In case of current domination this results in down-current oriented bars. When the conditions become more wave-dominated, the orientation of the bar changes to an up-current orientation. Hence the additional forcing of the hydrodynamics by the perturbations in radiation stresses due to bed and water level perturbations results in a rotation of the bar. The results obtained in the current-dominated regime, namely, the small spacing and the down-current orientation of the inner bar, corresponds very well with the findings of *Falquès et al.* [1996].

[85] In section 3.1.3 the sensitivity of the results to the sediment stirring function is discussed as well. In case of wave-dominated conditions, the cross-shore gradient of the potential stirring function is, despite the fact that  $\alpha$  is increasing with increasing  $x$ , negative. When considering current-dominated conditions, the cross-shore gradient of the potential stirring function is positive. Since the flow  $u'_c$  over a shoal ( $h' > 0$ ) is always onshore directed, independent of the hydrodynamic conditions, the shoal will erode under wave-dominated conditions but grow when considering a current-dominated sediment stirring. Using this observation and equation (24), it can be understood that for wave-dominated sediment stirring the growth rate increases with increasing wavelength although it is always negative: The cross-shore velocity is always negative over a shoal in the surf zone, but  $u'_c \rightarrow 0$  for  $\lambda \rightarrow \infty$ . Since  $\omega_i \propto \partial h'/\partial t \propto u'_c$ , it is clear that the growth rate goes to zero as  $\lambda \rightarrow \infty$ .

[86] The orientation of the bed perturbations found with the model described in section 2.2 is always up-current for the fastest growing bed forms. In the work of *Ribas et al.* [2003] it is argued that because of current refraction, down-current oriented bars are expected to have larger growth rates than up-current oriented bars. However, this argument is based on the assumption that the rotational component of the velocity field is negligible and a good description of the velocities is given by the potential component. This is, for example, the case in the work of *Calvete et al.* [2001]; see *Trowbridge* [1995] as well. However, in our case the rotational part of the velocity field is not necessarily negligible and hence the above argument cannot be applied in the surf zone. Consequently, the perturbations in the radiation stresses play a crucial role.

[87] A number of other results have been found with the idealized model that are not found in previous models such as that of *Ribas et al.* [2003]. In the work by *Ribas et al.* [2003] the bed slope and the drag coefficient are not studied separately. However, the results with the idealized model show that these parameters should be considered separately; see Figure 8. Changing the bed slope with constant drag coefficient results in different FGM. Second, Figure 8 shows that the spacing increases with increasing angle of wave incidence, which is opposite to the findings of *Ribas et al.* [2003], who find decreasing spacing with increasing angle of wave incidence, up to a certain angle beyond which the

**Table 2.** Relative Importance of the Various Components of the Divergence of the Sediment Flux to the Total Bed Change<sup>a</sup>

	$\theta_b = 5^\circ$ $\lambda = 500$ m	$\theta_b = 5^\circ$ $\lambda = 2500$ m
$q_{c,x}^x$	0.01	$<10^{-3}$
$q_{w,x}^x$	1.00	0.75
$q_{c,y}^y$	0.40	0.08
$q_{w,y}^y$	0.01	$<10^{-3}$

<sup>a</sup>All terms are scaled with  $q_{w,x}^x$  found for a wavelength  $\lambda = 500$  m.

spacing does not increase further with increasing angle of wave incidence.

#### 4.2. Fully Nonlinear Model

[88] Using the fully nonlinear model with an *Engelund and Hansen* [1967] transport formula, very oblique down-current oriented bars are found. The growth rate increases from negative values for small wavelengths to positive growth rates for large wavelengths, but a maximum growth rate is never found. The orientation of the bars becomes more and more oblique with increasing wavelength (and thus with increasing growth rate). Including bed slope effects, changing the angle of wave incidence, the bed slope or the drag coefficient does not qualitatively change these results. No FGM is found.

[89] To understand the absence of a FGM in the experiments done with the fully nonlinear model coupled to the *Engelund and Hansen* [1967] transport formula, the divergence of the sediment flux is subdivided in four components, namely,  $q_{c,x}^x$ ,  $q_{c,y}^y$ ,  $q_{w,x}^x$  and  $q_{w,y}^y$ . Here  $\vec{q}_c$  ( $\vec{q}_w$ ) denotes the sediment flux transported in the direction of the mean current (wave orbital velocity), the superscript denotes the component of the sediment flux in the cross-shore ( $x$ ) and longshore ( $y$ ) direction, and the subscripts  $x$  and  $y$  denote differentiation with respect to the cross-shore and longshore coordinate, respectively. The relative importance of the different terms to the total bed change is summarized in Table 2.

[90] From Table 2 and the comparison of the numerical experiments with and without sediment transport in the wave orbital direction, it is evident that divergences of the sediment flux in the wave orbital direction are crucial to have growing bed features. Since a positive growth rate is found for  $\lambda = 2500$  m and  $q_{w,y}^y$  is negligible compared to  $q_{w,x}^x$ , it is the latter contribution that is crucial for having positive growth rates. For a wavelength of  $\lambda = 500$  m, negative growth rates are found even though  $q_{w,x}^x$  gives the largest contribution to the divergence of the sediment flux. Note that this contribution is larger than the contribution found for a wavelength of 2500 m. Hence  $q_{c,y}^y$ , the only other significant term to the bed change, must have a damping effect. Since the magnitude of both  $q_{w,x}^x$  and  $q_{c,y}^y$  decrease with increasing wavelength, but the latter decreases faster than the former, it can be understood that the growth rate increases with increasing wavelength.

[91] Allowing for sediment transport in the current direction, only, results in up-current bars with a negative growth rate. It is instructive to compare the results of the fully nonlinear model with transport according to *Engelund and Hansen* [1967] in the current direction only with the results obtained with the idealized model forced with HISWA and

the equilibrium stirring function  $\alpha_c^{\text{wd}}$  derived from the fully nonlinear model. In both experiments the growth rates are negative and tend to zero for increasing wavelength. However, in case of the idealized model the bars are decaying, down-current oriented bars, whereas the fully nonlinear model results in decaying, up-current oriented bars. The remaining model differences between these experiments are (1) the stirring function in the fully nonlinear model experiments that depends on the longshore coordinate, while it is longshore-uniform in the idealized experiment and (2) the nonlinear bottom friction used in the fully nonlinear model formulation versus the linearized bottom friction in the idealized model. Previous results [see *Klein and Schuttelaars*, 2004] indicate that the difference in orientation is mainly due to differences in the stirring function.

[92] From the experiments it can be deduced that the obliqueness increases with increasing wavelength. For  $\lambda \rightarrow \infty$  the bed perturbations become shore-parallel. From the analysis above it is clear that all terms vanish except  $q_{w,x}^x$ , the term that is responsible for the growth. This suggests that for increasing wavelength the growth rate continuously increases to a certain limit value  $\omega_i^\infty$ .

[93] Applying the *Bailard* [1981] transport formula, growing up-current oriented bed forms are obtained for wave angles smaller than approximately  $7^\circ$ . No preferred wavelength is found in the range of the wavelengths considered. A few additional experiments including bed slope effects have been performed but also these experiments do not yield a FGM for a wavelength larger than 300 m, although the growth rates of the modes with small wavelength are more reduced by bed slope effects than modes with larger wavelengths.

[94] Taking only bed load or suspended load into account growing, up-current bed forms are found, although the eigenvalues are modified. When omitting the bed and suspended load in the direction of the wave orbital velocity from the *Bailard* [1981] formulations, only stable, up-current bed forms are found. Hence sediment transport in the direction of the wave orbital motion is crucial for growing bed forms. In more detail, bed load transport in the direction of the wave orbital motion is sufficient to have an unstable system.

[95] For angles of wave incidence larger than  $7^\circ$  the results of the LSA obtained with the method of *Bailard* [1981] are very similar to the results obtained by *Engelund and Hansen* [1967]. Very oblique down-current bars with positive growth rates are obtained for large wavelengths. For small wavelengths, contrary to *Engelund and Hansen* [1967], up-current bars with negative growth rates are found. The results obtained with both the *Engelund and Hansen* [1967] and *Bailard* [1981] transport formulations show that neglecting the contribution of the sediment transport in the direction of the waves, only bed perturbations with negative growth rates are found.

## 5. Conclusions

[96] In this paper, the sensitivity of the linear stability characteristics of planar beaches to parameter values and process formulations is determined using a fully nonlinear model and an idealized version of it. Applying the idealized model, the fastest growing bed perturbation consists of a

crescentic pattern with a slightly up-current oriented inner bar, migrating in the direction of the mean longshore current. From the results of the idealized model it is evident that the spacing and the growth and migration rates depend strongly on the bed slope, the drag coefficient and the angle of wave incidence. Independent of the angle of wave incidence or the drag coefficient, a maximum growth rate and a minimum spacing are found for a bed slope of approximately 1%. These maxima and minima become more pronounced with increasing current-dominance.

[97] In the limit of the current-dominated regime ( $\gamma_{cw} = 1$ ), the resulting bed perturbations are alternating channels and shoals around the breaker line, with the inner bar being down-current oriented with small preferred spacings (<300 m). These results are very similar to the results of *Falqués et al.* [1996] and stress the importance of a correct formulation of the forcing terms.

[98] To assess the importance of irregular waves and wave refraction with respect to the perturbed bathymetry, the wave forcing is calculated using HISWA. This information is used to drive the velocities in the idealized model. The sediment stirring  $\alpha(x)$  is still prescribed and not calculated using the information from the wave model. Although the spatial structure remains approximately the same, the fastest growing perturbation has a much smaller wavelength compared to the experiments in which the wave forcing is prescribed according to *Longuet-Higgins* [1970]. Furthermore, both the growth and migration rate become smaller.

[99] To evaluate the importance of the stirring function itself, the stirring function is calculated using both the current and orbital velocities obtained in morphodynamic equilibrium. Hence the stirring function used in these experiments is longshore-uniform and is not perturbed in this experiment. Using this formulation, the bed forms are down-current oriented and have negative growth rates. Note that the bed forms obtained using a prescribed wave stirring function are up-current oriented and growing in time. This indicates that a good parameterization of the wave-stirring function is essential to model the bar behavior in the surf zone correctly.

[100] When using the fully nonlinear model with the *Engelund and Hansen* [1967] transport formula, growing bed perturbations are found consisting of very oblique down-current oriented bars. The growth rate increases from negative values for small wavelengths to positive growth rates for large wavelengths, but a maximum growth rate is never found. The orientation of the bars becomes more and more oblique with increasing wavelength. Including bed slope effects, changing the angle of wave incidence, the bed slope or the drag coefficient does not qualitatively change these results. When the sediment transport in the direction of the wave orbital velocity is neglected, the growth rates of all bed perturbations are negative and tend to zero for increasing wavelength. The bed perturbations are up-current oriented bars. These results can be compared with the results of the idealized model forced with the HISWA wave model and a fully nonlinear, but longshore-uniform sediment stirring function, that results in bars with a negative growth rate and down-current orientation. In case of the idealized model the bars are decaying but down-current oriented. This difference in bar orientation is related to the

neglect of the longshore variation of stirring function in the idealized model experiment.

[101] When the *Bailard* [1981] sediment transport formula is used instead of the *Engelund and Hansen* [1967] formula, fastest growing bed perturbations are found for  $\theta_b < 7^\circ$ , although the wavelength of the FGM is smaller than the minimum wavelength that could be assessed. The bed forms are up-current oriented bars. When neglecting the sediment transport in the direction of the waves, no growing bed forms are found. For larger angles the results of the LSA are very similar to the results obtained by *Engelund and Hansen* [1967], namely, mainly decaying, very oblique down-current bars with the growth rates increasing with the wavelength. The magnitude of the growth rates is in that case of the same order of magnitude as the growth rates obtained by *Engelund and Hansen* [1967].

[102] Hence from the fully nonlinear model results it can be concluded that to have linearly growing bed perturbations, it is essential to take the transport in the direction of the wave orbital velocity into account. If only the transport in the current direction is taken into account and a physically feasible sediment stirring function is used, all bed perturbations decay.

[103] In this paper we have shown that the linear growth of bed perturbations on top of a planar beach is highly sensitive to model formulations and, to a lesser extent, to parameter values. The results are especially sensitive to the sediment transport formulation. Not only the variation of the results obtained in this paper is large, but also many differences with and between results reported in the literature learn us that linear stability analyses of planar beaches as a predictive tool for bed forms in the finite amplitude domain should be used with care.

[104] This conclusion is supported by findings of *Klein et al.* [2004] and M. D. Klein and H. M. Schuttelaars (Morphodynamic evolution of double-barred beaches, submitted to *Journal of Geophysical Research*, 2005) (hereinafter referred to as Klein and Schuttelaars, submitted manuscript, 2005) for barred beaches. In the work of *Klein et al.* [2004] it was shown that the linear stability characteristics of barred beaches are far much less sensitive to the sediment transport formulation, although significant differences between the preferred spacings obtained with *Engelund and Hansen* [1967] and *Bailard* [1981] exist. The predictive capabilities of linear stability analyses of barred beaches for the temporal evolution of these beaches and a comparison with observations is made by Klein and Schuttelaars (submitted manuscript, 2005), showing that the results of the LSAs are only a good prediction of the bed forms and their orientation, length scales and migration rates in the initial phase of the temporal evolution.

[105] However, linear stability analyses are very suitable to understand basic mechanisms. Especially the BEE, introduced by *Falqués et al.* [1996], is a powerful tool. It gives an explanation for the sign of the growth rate and the structure of the bed perturbation, given cross-shore bed profile, a perturbed velocity field and a sediment stirring function. On a planar beaches, the ratio between the bed profile and the wave stirring function is delicate, explaining some of the variation in the results presented in this paper and the literature. It also explains the fact that the linear stability characteristics of barred beaches are much less

sensitive to the sediment transport formulation, since the bed profile has already a large gradient in itself and thereby dominates the potential stirring function of the BEE.

[106] **Acknowledgments.** The research presented herein is done in the frame work of the DIOC-programme "Water" of Delft University of Technology. H. M. Schuttelaars' contribution was supported by NWO-ALW grant 810.63.12. The authors wish to thank Johan van der Molen for kindly making his sediment transport routines available. The authors also wish to thank Huib de Swart, Ad Reniers, Francesca Ribas, Albert Falqués and the two anonymous reviewers for their thorough reviews and useful comments.

## References

- Bailard, J. A. (1981), An energetics total load sediment transport model for a plane sloping beach, *J. Geophys. Res.*, 86(C11), 10,938–10,954.
- Battjes, J. A., and J. P. F. M. Janssen (1978), Energy loss and set-up due to breaking in random waves, paper presented at 16th International Conference on Coastal Engineering, Am. Soc. of Civ. Eng., New York.
- Battjes, J. A., and M. J. F. Stive (1985), Calibration and verification of a dissipation model for random breaking waves, *J. Geophys. Res.*, 90(C5), 9159–9167.
- Bowen, A. J., and D. L. Inman (1971), Edge waves and crescentic bars, *J. Geophys. Res.*, 76(36), 8662–8671.
- Caballeria, M., G. Coco, A. Falqués, and D. A. Huntley (2002), Self-organisation mechanics for the formation of nearshore crescentic and transverse sand bars, *J. Fluid Mech.*, 465, doi:10.1017/S002211200200112X, 379–410.
- Calvete, D., A. Falqués, H. E. de Swart, and M. Walgreen (2001), Modelling the formation of shoreface-connected sand ridges on storm dominated inner shelves, *J. Fluid Mech.*, 441, 169–193.
- Chen, Y., and R. T. Guza (1998), Resonant scattering of edge waves by longshore periodic topography, *J. Fluid Mech.*, 369, 91–123.
- Christensen, E. D., R. Deigaard, and J. Fredsøe (1994), Sea bed stability on a long straight coast, paper presented at 24th International Conference on Coastal Engineering, Am. Soc. of Civ. Eng., New York.
- Deigaard, R., N. Drønen, J. Fredsøe, J. H. Jensen, and M. P. Jørgensen (1999), A morphological stability analysis for a long straight barred coast, *Coastal Eng.*, 36, 171–195.
- Dingemans, M. W., A. C. Radder, and H. J. de Vriend (1987), Computations of driving forces of wave-induced currents, *Coastal Eng.*, 11, 539–563.
- Dodd, N. (1994), On the destabilization of a longshore current on a plane beach: Bottom shear stress, critical conditions, and onset of instability, *J. Geophys. Res.*, 99(C1), 811–824.
- Dyer, K. R., and D. A. Huntley (1996), The origin, classification and modelling of sand banks and ridges, *Cont. Shelf Res.*, 19, 1285–1330.
- Engelund, F., and E. Hansen (1967), *A Monograph on Sediment Transport in Alluvial Streams*, Technisk Forlag, Copenhagen.
- Falqués, A., and D. Calvete (2003), Propagation of coastline sand waves, paper presented at 3rd Symposium on River, Coastal and Estuarine Morphodynamics, Int. Assoc. for Hydraul. Res., Barcelona, Spain.
- Falqués, A., A. Montoto, and V. Iranzo (1996), Bed-flow instability of the longshore current, *Cont. Shelf Res.*, 16, 1927–1964.
- Falqués, A., G. Coco, and D. A. Huntley (2000), A mechanism for the generation of wave-driven rhythmic patterns in the surf zone, *J. Geophys. Res.*, 105(C10), 24,071–24,087.
- Fredsøe, J. (1984), Turbulent boundary layer in wave-current motion, *J. Hydraul. Eng.*, 110, 1103–1120.
- Griffel, D. H. (1985), *Applied Functional Analysis*, Ellis Horwood Limited, Chichester, UK.
- Hino, M. (1974), Theory on formation of rip-current and cuspidal coast, *Proceedings of the 14th International Conference on Coastal Engineering*, pp. 901–919, Am. Soc. of Civ. Eng., New York.
- Holman, R. A., and A. J. Bowen (1982), Bars, bumps, and holes: Models for the generation of complex beach topography, *J. Geophys. Res.*, 87(C1), 457–468.
- Holthuijsen, L. H., N. Booij, and T. H. C. Herbers (1989), A prediction model for stationary, short-crested waves in shallow water with ambient currents, *Coastal Eng.*, 13, 23–54.
- Horikawa, K. (1999), *Nearshore Dynamics and Coastal Processes*, Univ. of Tokyo Press, Tokyo.
- Klein, M. D., and H. M. Schuttelaars (2004), Influence of bed slope and friction on the linear stability of planar beaches, paper presented at Marine Sandwave and River Dune Dynamics II, Univ. of Twente, Enschede, Netherlands.
- Klein, M. D., H. M. Schuttelaars, and M. J. F. Stive (2002), Linear stability of a double-barred beach, paper presented at 28th International Conference on Coastal Engineering 2002, Am. Soc. of Civ. Eng., New York.
- Klein, M. D., H. M. Schuttelaars, and M. J. F. Stive (2004), Influence of sediment transport formulation on linear stability of planar and barred coasts, paper presented at 29th International Conference on Coastal Engineering 2004, Am. Soc. of Civ. Eng., New York.
- Konicki, K. M., and R. A. Holman (2000), The statistics and kinematics of transverse sand bars on an open coast, *Mar. Geol.*, 169, 69–101.
- Longuet-Higgins, M. S. (1970), Longshore currents generated by obliquely incident sea waves: 1, *J. Geophys. Res.*, 75(33), 6778–6789.
- MacMahan, J. H., A. J. H. M. Reniers, E. B. Thornton, and T. P. Stanton (2004), Infragravity rip current pulsations, *J. Geophys. Res.*, 109, C01033, doi:10.1029/2003JC002068.
- Phillips, O. M. (1977), *The Dynamics of the Upper Ocean*, Cambridge Univ. Press, New York.
- Reniers, A. J. H. M., J. A. Roelvink, and E. B. Thornton (2004), Morphodynamic modeling of an embayed beach under wave group forcing, *J. Geophys. Res.*, 109, C01030, doi:10.1029/2002JC001586.
- Ribas, F., A. Falqués, and A. Montoto (2003), Nearshore oblique sand bars, *J. Geophys. Res.*, 108(C4), 3119, doi:10.1029/2001JC000985.
- Roelvink, J. A., and G. K. F. M. van Banning (1994), Design and development of Delft3D and application to coastal morphodynamics, in *Hydroinformatics '94 Conference*, pp. 451–455, Balkema, Rotterdam.
- Sonu, C. J. (1968), Collective movement of sediment in littoral environment, paper presented at 11th International Conference on Coastal Engineering, Am. Soc. of Civ. Eng., New York.
- Soulsby, R. L., L. Hamm, G. Klopman, D. Myrhaug, R. R. Simons, and G. P. Thomas (1993), Wave-current interactions within and outside the bottom boundary layer, *Coastal Eng.*, 21, 41–69.
- Stive, M. J. F., et al. (2002), Variability of shore and shoreline evolution, *Coastal Eng.*, 47, 211–235.
- Terwindt, J. H. J. (1971), Sand waves in the Southern Bight of the North Sea, *Mar. Geol.*, 10, 51–67.
- Trowbridge, J. H. (1995), A mechanism for the formation and maintenance of shore-oblique sand ridges on storm-dominated shelves, *J. Geophys. Res.*, 100(C8), 16,071–16,086.
- Van de Meene, J. W. H., and L. C. van Rijn (2000), The shoreface-connected ridges along the central Dutch coast: Part 1. Field observations, *Cont. Shelf Res.*, 20, 2295–2323.
- Van der Molen, J. (2002), The influence of tides, wind and waves on the net sand transport in the North Sea, *Cont. Shelf Res.*, 22, 2739–2762.
- Van Enckevort, I. M. J., and B. G. Ruessink (2003), Video observations of nearshore bar behaviour: Part 2. Alongshore non-uniform variability, *Cont. Shelf Res.*, 23, 513–532.
- Van Enckevort, I. M. J., et al. (2004), Observations of nearshore crescentic sandbars, *J. Geophys. Res.*, 109, C06028, doi:10.1029/2003JC002214.
- Verhagen, H. J. (1989), Sand waves along the Dutch coast, *Coastal Eng.*, 13, 129–147.
- Wright, L. D., and A. D. Short (1984), Morphodynamic variability of surf zones and beaches: A synthesis, *Mar. Geol.*, 56, 93–118.

M. D. Klein and H. M. Schuttelaars, Section of Hydraulic Engineering, Delft University of Technology, P.O. Box 5048, 2600 GA Delft, Netherlands. (m.d.klein@ct.tudelft.nl)